Seismic stratigraphy of Cretaceous eastern Central Atlantic Ocean: Basin evolution and palaeoceanographic implications

Yannick Mourlot, Gérôme Calvès, Peter D. Clift, Guillaume Baby, Anne-Claire Chaboureau, François Raisson

Elsevier Editorial System(tm) for Earth and Planetary Science Letters

Manuscript Draft

Manuscript Number: EPSL-D-18-00035R1

Title: SEISMIC STRATIGRAPHY OF CRETACEOUS EASTERN CENTRAL ATLANTIC OCEAN: BASIN EVOLUTION AND PALAEOCEANOGRAPHIC IMPLICATIONS

Article Type: Letters

Keywords: Seismic reflection, contourite, palaeobathymetry, palaeoceanography, Cretaceous, Central Atlantic Ocean.

Corresponding Author: Dr. GEROME CALVES, Ph.D.

Corresponding Author's Institution: UNIVERSITE TOULOUSE 3

First Author: Yannick Mourlot, Ph.D.

Order of Authors: Yannick Mourlot, Ph.D.; GEROME CALVES, Ph.D.; Peter D Clift, Ph.D.; Guillaume Baby, Ph.D.; Anne-Claire Chaboureau, Ph.D.; François Raisson, MSc

Abstract: The evolution and resulting morphology of a Cretaceous contourite drift in the eastern Central Atlantic oceanic basin is investigated in unprecedented detail using seismic imaging and age-calibrated cross-margin sections. The margin, from the shelf, slope to deep-water and abyssal plain is constructed by a succession of erosive and depositional mounded structures that relate to bottom-water currents and sediment winnowing. The regional mapping of these drifts, sediment waves and gravitational sedimentary systems allows us to test the Upper Cretaceous paleocirculation model. Combined with flexural backstripping of the regional cross section, it reveals the water-depth range at which the observed sedimentary features occur. A possible late Albian to Turonian contourite drift system is observed from Guinea to Mauritania. The development of a shallow to deep oceanic circulation system is a key element in the rock record, with implications for the palaeoceanography and layering of the Cretaceous ocean. The Cretaceous geological interval and oceanic model mirrors the stratification of the modern ocean and the morphology of its seafloor from offshore Morocco to Guinea.

Highlights :

- Morphology and evolution of a Cretaceous contourite drift in the eastern Central Atlantic oceanic basin

- Backstripping of the regional cross section reveals the water-depth range at which the observed sedimentary features occur

- Cretaceous geological interval and oceanic model mirrors the stratification of the Modern Ocean and the morphology of its seafloor

SEISMIC STRATIGRAPHY OF CRETACEOUS EASTERN CENTRAL ATLANTIC OCEAN: BASIN EVOLUTION AND PALAEOCEANOGRAPHIC IMPLICATIONS

Yannick Mourlot[1], Gérôme Calvès[1,*], Peter D. Clift[2], Guillaume Baby[1], Anne-Claire Chaboureau[3], François Raisson[4]

[1] Université Toulouse 3, GET–OMP, 14 Avenue Edouard Belin, 31400, Toulouse, France (*corresponding author: gerome.calves@get.omp.eu)

[2] Department of Geology and Geophysics and Coastal Studies Institute, E235 Howe-Russell, Louisiana State University, Baton Rouge, Louisiana 70803, USA

[3] CVA, 7 chemin de la Marouette, 64100 Bayonne, France

[4] Total E&P, CSTJF, Avenue Larribau, F–64018, Pau Cedex, France

Keywords: Seismic reflection, contourite, palaeobathymetry, palaeoceanography, Cretaceous, Central Atlantic Ocean.

ABSTRACT

The evolution and resulting morphology of a Cretaceous contourite drift in the eastern Central Atlantic oceanic basin is investigated in unprecedented detail using seismic imaging and age-calibrated cross-margin sections. The margin, from the shelf, slope to deep–water and abyssal plain is constructed by a succession of erosive and depositional mounded structures that relate to bottom-water currents and sediment winnowing. The regional mapping of these drifts, sediment waves and gravitational sedimentary systems allows us to test the Upper Cretaceous paleocirculation model. Combined with flexural backstripping of the regional cross section, it reveals the water-depth range at which the observed sedimentary features occur. A possible late Albian to Turonian contourite drift system is observed from Guinea to Mauritania. The development of a shallow to deep oceanic circulation system is a key element in the rock record, with implications for the palaeoceanography and layering of the Cretaceous ocean. The Cretaceous geological interval and oceanic model mirrors the stratification of the modern ocean and the morphology of its seafloor from offshore Morocco to Guinea.

1. Introduction

The sedimentary architecture of passive margins is generally shaped by both gravitational processes (*e.g.* turbidites, debris flows) and along–slope oceanic bottom currents (contourite drifts) (*e.g.* Rebesco et al., 2017). The modern ocean seafloor records the interaction between surface and deep bottom-water currents through their expression in the erosion and deposition of sediments (Heezen and Hollister, 1964). Features such as mounded contourite drifts mark some of the most extensive expression of interactions between sediment and water masses across the seafloor of modern oceanic sedimentary basins (Faugères et al., 1999; Stow et al., 2002; Mosher et al., 2017). The acquisition of seafloor photography, subsurface seismic reflection profiles and the sampling of marine sediments has allowed the identification of sediment transport by bottom-water currents in various bathymetric domains (*e.g.* abyssal plain and shelf). This is particularly well known in the Atlantic, Pacific and Indian Oceans (Faugères et al., 1999; Hernández–Molina et al., 2008a and b; Rebesco et al., 2014).

During the Cretaceous, palaeoceanographic circulation patterns in the Tethys, Atlantic, Indian and Pacific Oceans have been inferred from the tracking of oceanic water masses using the neodymium (Nd) isotope character of fish teeth. In addition, global and regional modeling combining atmospheric and oceanic circulation has been performed to illustrate possible ocean circulation patterns and specify water mass exchanges between the different oceans (Poulsen et al., 2001; Donnadieu et al., 2016; Uenzelmann–Neben et al., 2016). However, these simulations could not resolve the full water column stratification because they investigated the surface and intermediate oceanic currents without any constraints on the paleo-seafloor and its interaction with deep bottom-water currents.

Studies based on Nd isotope character of Upper Cretaceous fish teeth sampled in the Equatorial Atlantic domain (MacLeod et al., 2008; Martin et al., 2012) propose two intermediate oceanic currents: a first one originating in the Demerara Rise region (Demerara

Bottom Water: DBW, Figure 1) and a second initiating from the South Atlantic Ocean and circulating toward the Central Atlantic Ocean through the Equatorial Gateway (Southern Component Waters: SCW, Figure 1) (Robinson and Vance, 2012). Other studies, also based on Nd isotopes, assume that in the northern Central Atlantic Ocean, a surface current originating in the Tethys Ocean would have run through the Central Atlantic to the lowest latitudes (Northern Component Waters: NCW, Figure 1) (Pucéat et al., 2005; MacLeod et al., 2008). However, these Upper Cretaceous large-scale ocean circulation patterns remain debated because recent studies have emphasized the importance of paleobathymetric obstacles. Indeed, critical topographic barriers could have limited connections between the ocean basins, forcing water masses to evolve in more restricted areas (Voigt et al., 2013; Uenzelmann–Neben et al., 2016).

The present day water column in the eastern Central Atlantic Ocean is stratified into the following layers: shallow (0–500 m depth, *e.g.* South Atlantic Central Water – SACW), intermediate (500–1500 m depth, *e.g.* Antarctic Intermediate Water – AIW) and deep (1500 m–seafloor, *e.g.* Antarctic Bottom Water – ABW) water masses (Emery and Meincke, 1986). The present day shallow subsurface oceanic layers have been also well studied by the oceanographic and marine geology communities. Many sedimentary structures related to bottom-water currents and gravity-driven processes have been identified on the modern seafloor along the Northwest African Margin between Morocco and Mauritania (*e.g.* Wynn et al., 2000; Schwab et al., 2007). In contrast to these well documented features related to modern bottom-water currents, only a few examples of Cretaceous sedimentation related to bottom current processes are found. These studies are restricted to the northern Central Atlantic Ocean (Morocco: Dunlap et al., 2013; Northwest Iberia: Soares et al., 2014). Between 24° and 8° N from the Western Sahara to Guinea (Figure 1) the authors found no

studies that document Cretaceous sedimentation in relation to processes that involve interaction between the seafloor and deep bottom currents.

This study aims at understanding the occurrence of specific sedimentary features present in the deep-sea Cretaceous Ocean record and their implication for the oceanic circulation. This paper uses 2D seismic reflection profiles, borehole data from Deep Sea Drilling Project (DSDP) Sites 367 and 368 located along the Northwest African margin.

We document a variety of sedimentary features observed over a range of palaeobathymetry from the continental shelf, the slope to the deep abyssal plain during the Cretaceous. We also quantify paleobathymetric domains both in the shelf and the deep basin using flexural decompaction of regional geological sections where we have observed bottom-water current-related sedimentary features. These new results allow to understand deep-water oceanic circulation in the eastern Central Atlantic Ocean during the Cretaceous.

2. Data and Methods

2.1. Seismic stratigraphy

In this study, we use a combination of both 2D seismic sections and drilling data from the shallow to deep–water Central Atlantic margin (30°–10° N; Figure 1; Figure S1, Shipboard Scientific Party, 1978) to reconstruct the sedimentary architecture of this margin with the objective of better understanding the Upper Cretaceous palaeoceanography. The average spacing between lines is ~10 km with exception in the distal offshore domain where only regional lines exist. The margin is described with standard seismic stratigraphic techniques based on reflection terminations and seismic reflection facies, as well as the relationship to the geometry of individual seismic reflections (terminations). This approach allows the seismic profile to be divided into chronostratigraphic packages. Thus, eight seismic surfaces were used to define seven seismic units in the studied interval. An age calibration was obtained

using well data (*e.g.* Hardenbol et al., 1981; Davison, 2005; see Table 1; Figures 1 and 2). These data provide important evidence for the timing of formation and the distribution of several sedimentary features related to channel-levees, deep-sea fans and mass transport complexes (Posamentier and Kolla, 2003). The data are also used to understand sediment remobilization by bottom ocean currents (*e.g.,* contourite drift) in both the basin and the slope (Faugères et al., 1999; Stow et al., 2002). Seismic reflection horizons, interpreted in the travel-time domain, to provide a seismic stratigraphic framework were depth-converted using a combination of velocities based on geophysical methods (sonobuoy records, check-shot) and regional isopach maps or depth cross-section from long–offset seismic records. Time-depth data and the depth conversion equation can be found in the supplementary files (Figure S2).

2.2. Mesozoic stratigraphy of the eastern Central Atlantic Ocean

In the Senegal and Mauritania basins, DSDP Sites 367 and 368 sampled the post–rift Mesozoic stratigraphic sequences of the deep ocean basin (Figures 1 and 2). DSDP Site 367 shows that the basalts of the oceanic crust are overlain by a Jurassic to Lower Cretaceous sedimentary unit consisting of interbedded limestone with marl and cherts (Figure 2, Lancelot et al., 1978a). These lithological units were deposited in a bathyal pelagic environment with the presence of clastic deposits input by turbidity currents during the Lower Cretaceous (Jansa et al., 1978). The Barremian to Aptian sequence comprises alternating limestone with marl and thin black shale. This shalier unit progressively grades into thick black shale deposits from the transition between the Barremian and the Aptian, as observed at DSDP Sites 367 and 368. These black shales are platform material remobilized by turbidity currents and deposited in the abyssal plain (Lancelot et al., 1978a; Jansa et al., 1978). The increase in proportion of shale during the Lower Cretaceous is also evidenced by drilling results at DSDP Site 398 in the northern Central Atlantic Ocean (Northwest Iberia). Soares et al. (2014) observed

contourite drifts and sediment waves on seismic reflection profiles at this location (Figure 2). The Albian to Upper Cretaceous sequence, deposited in a similar environment as during the Aptian, is composed of dominant black shale facies interbedded with more silty, less shaly layers, as illustrated in DSDP Sites 367 and 368 (Figure 2). This lithology is different from that found at DSDP Site 398 where Upper Cretaceous formations correspond to limestone interbedded with claystone and marl units (Figure 2, Ryan et al., 1979). Cenozoic diabase sills intruded the Albian to Turonian black shales at DSDP Site 368. In the area of DSDP Sites 367 and 368, the Cretaceous sequence is of particular interest because it comprises turbidites deposited as a result of remobilization (Jansa et al. 1978).

2.3. Backstripping and paleobathymetric estimates

The aim of our backstripping study is to give constraints on the paleobathymetric range of deposition of contourite drift deposits that are observed in the deeper and distal parts of the margins. In these locations, there are limited or no core samples that allow calibration of absolute value of bathymetry. For this analysis, we use a flexural backstripping approach that has been used in various geological settings to infer paleodepth down to basement in sedimentary basins and to reconstruct vertical movements (*e.g.* Clift et al., 1995; Calvès et al., 2008). Subsidence of the study area has been investigated in two sedimentary basins: (1) to the north of the margin in the Aaiun Basin (Morocco) linked to DSDP Site 397 (von Rad and Einsele, 1980), and, (2) to the south in the Senegal Basin (Latil–Brun and Lucazeau, 1988). The studied stratigraphic interval is characterized by normal post-rift thermal subsidence (von Rad and Einsele, 1980; Latil–Brun and Lucazeau, 1988). The investigated period and study area has been calibrated with a thermal subsidence corresponding to a coefficient of extension of 1.2 (Latil–Brun and Lucazeau, 1988). This factor has been set as an input in the backstripping computation. The 2D backstripping method is a standard basin analysis

149 approach, with numerous published results attesting that this particular method is robust
150 within the limits of the approach (*e.g.* Kusznir et al., 1995; Roberts et al., 1998).
151 In detail, the first step is the removal of the present-day water column covering the
152 whole section leading to the computation of the flexural isostatic response specific to this
153 removal. Then, the uppermost sedimentary layer (initially overlain by the water column) is
154 also removed from the section. This involves the decompaction of underlying sediments in
155 response to this removal and unloading, which is computed by the software from the physical
156 parameters of the remaining sedimentary units (*i.e.* lithology, density and porosity, Table 1).
157 The 2D backstripping method provides several restored 2D–sections, which can be also
158 corrected by the flexural strength of the lithosphere commonly expressed by the effective
159 elastic thickness (T_e, in km). This parameter expresses the thickness of a perfectly elastic layer
160 with similar flexural properties to the lithosphere (*e.g.* Watts, 1978). Low values of effective
161 elastic thickness (<5 km) illustrate a weak lithosphere which suffers from deformation
162 because of the flexural isostatic response of the sedimentary load variation. In contrast, a high
163 value of T_e (> 15 km) represents a strong lithosphere which is affected by moderate or low
164 deformation during the flexural isostatic response of the sedimentary load (*e.g.* Roberts et al.,
165 2009). The elastic thickness in the studied area has been estimated with the global *Te* grid
166 map (*e.g.* Watts, 2015; Global T_e grid: ftp://ftp.earth.ox.ac.uk/pub/tony/TOG/global_te.grd).
167 The continental and oceanic T_e values from the study area are compiled in the supplementary
168 data. The median T_e value for the oceanic domain is 26.6 km (s.d.: 6.6) and for the continental
169 areas 17.5 km (s.d.: 8.7) (see supplementary files: Figure S2). We used different values of T_e
170 (0, 10, 20 and 30 km) to compute paleobathymetric ranges depending on the flexural rigidity
171 of the plate.

172 **3. Results**

173 3.1. Margin geometry

174 The present–day structure of the Northwest African margin is well documented (*e.g.* Emery
175 and Uchupi, 1984). It is composed of four sedimentary basins between Morocco and Sierra
176 Leone (Figure 1) which are dominated by a large and flat continental shelf (>100 km) with a
177 maximum water depth of 200 m (*e.g.* Senegal Shelf, Figures 3 and 4, Wynn et al., 2000;
178 Davison, 2005). Offshore Morocco and Mauritania, the shelf becomes narrower and is
179 affected by salt tectonics and volcanism (von Rad et al., 1982). Two E–W sections, one N–S
180 section and one NW–SE section have been selected to illustrate the geometry of the margin
181 and its evolution from the Jurassic to the Upper Cretaceous offshore Mauritania, Senegal and
182 Guinea (Figures 3 and 4). Offshore Mauritania, the E–W profile illustrates the Jurassic
183 sequence that has a maximum extent of 200 km in width and a maximum thickness of 2.5 km
184 in the basin (Figures 3A and B). This sequence is thicker under the shelf (up to 5 km of
185 thickness, Figure 3B). This Tethyan-type carbonate platform extends all around the Central
186 Atlantic domain (Emery and Uchupi, 1984). During the Cretaceous, slopes had a low gradient
187 (Figure 3B) and the sedimentary thickness thinned into the basin towards DSDP Site 368
188 (from 4.5 km to 1.5 km thick, Figure 3B).

189 In the Senegal E–W section (Figure 3C), the Jurassic sequence has a maximum thickness of 1
190 km in the deep basin and 3.5 km under the shelf, which is less than that observed offshore
191 Mauritania (Figure 3D). The paleo–slope was steep which is characteristic of a deep
192 carbonate bank margin, such as that of the modern Bahamas (Mullins and Neumann, 1979).
193 During the Cretaceous, the sedimentary pile accumulated a maximum thickness of 5 km in the
194 deep basin, that thinned further west, and reached <1 km thick at DSDP Site 367 (Figure 3D).
195 The paleo–slope remained steep during this period, consistent with a deep carbonate bank
196 margin geometry. An erosional surface (SU) is observed between 220 and 245 km along the
197 seismic reflection profile shown in Figure 3D. This surface is correlated to Senonian in age

198 and illustrates the absence of Albian to Upper Cretaceous sedimentary cover under in outer
199 shelf and the related slope.
200 The N-S section offshore Mauritania illustrates the structure of the Mauritanian Basin
201 between the shelf in the region of Ras Nouadhibou to the north and the shelf in the region of
202 Dakar to the south (Figure 4A). The profile shown in Figure 4A does not reach the base of the
203 Jurassic sequence. Nevertheless, the steep paleo–slope seen in the top Jurassic reflection
204 illustrates a typical carbonate-bank margin geometry in the region of Ras Nouadhibou
205 between 420 and 500 km along the seismic profile shown in Figure 4B. The Lower
206 Cretaceous sequence is thicker, up to 5 km, while the whole thickness of younger Cretaceous
207 units does not exceed a maximum of 2 km in this region (Figure 4B).
208 The NW-SE section offshore Guinea illustrates the geometry of the Guinean Plateau (Figures
209 4C and 4D). The Guinean Plateau forms a prominent corner between the Senegal and the
210 Sierra Leone basins (Figure 1). It corresponds to a submarine bathymetric high in ~700 m of
211 water-depth (Figure 4D). The base of the Jurassic could not be identified between 30 km and
212 160 km along this profile as the seismic data do not image to this depth (Figure 4C).
213 However, the Mesozoic unit (<6 km thick under the shelf and 3 km in the basin, Figure 4D) is
214 dominated by a Jurassic to the Cenomanian carbonate sequence from the. It turns into a mixed
215 carbonate/clastic regressive sequence in the Upper Cretaceous which remains thin (<0.5 km)
216 both under the plateau and in the basin (Figure 4D). Until the top of the Cenomanian, the
217 paleo–slope remains steep while it becomes gentler within the Upper Cretaceous and the
218 Cenozoic (Figure 4D).

219 3.2. Seismic facies and associated deposits

220 *3.2.1. Mounded seismic feature nearby DSDP Site 367 during Jurassic to Lower*
221 *Cretaceous*

The DSDP Site 367 (Figure 1, 3C and 5A) has been drilled on a thin sedimentary section located on top of a basement high. This high is standing at a shallow level below the seafloor, 1.121 sTWT mbsf, compared to the surrounding deeper part at ~1.61 sTWT mbsf to the east and 1.475 sTWT mbsf to the west in the deep basin (legacy seismic images are included in supplementary Figure S1; Shipboard Scientific Party and David Bukry, 1978). To the west of DSDP Site 367, the Lower Cretaceous sequence is thick (>620 m) compared to the east (400 m), and includes several moderate to high amplitude reflections that show onlap terminations on a positive topographic structure inherited from the underlying oceanic crust (Figure 5A). Within the lower Cretaceous sequence the main seismic facies is composed of well-stratified sub-parallel reflection with moderate to high amplitude and good lateral continuity (Figure 5A). A slight change of thickness is observed from the east to the west of DSDP Site 367. The Aptian sequence presents low to moderate amplitude reflections with terminations that onlap on the Lower Cretaceous thickened structure observed to the West of DSDP Site 367 (Figure 5B). The sequence thins above the Lower Cretaceous mounded structure and is associated to top lap terminations in its upper section. The slight decrease in thickness laterally, internal seismic facies, the low-mounded geometry, and the location above a structural high suggest that these features could be sheeted drifts. These sheeted drifts forms a sedimentary drape above the irregularities of the oceanic basement observed in many deep-water distal margins (Hernández–Molina, et al., 2008a). The moat surrounding these basement-tectonic controlled drift cannot be yet mapped here due to the low spatial seismic coverage.

3.2.2. Base of slope seismic facies during Cenomanian to Late Cretaceous

Two main seismic facies are observed at the base of slope of the NW African Margin. The first seismic facies consists of lenticular features with locally high amplitude reflections (HAR) packages within lower amplitude extensive continuous reflections packages (Figure 6A). These facies corresponds to deep-sea fans architectural elements that are the channel-

247 levees complexes, with the channel (HAR) and the overbank deposits and levees (e.g. Flood
248 et al., 1991)(Figure 6A). The deep-sea fan apex ends updip with onlap terminations on the
249 base of the continental slope (Figure 6A). Cretaceous deep-sea fan complexes observed in the
250 study area show a maximum thickness of 1 km over an average length of 60 km. Overall, they
251 are thicker at the foot of the continental slope and become gradually thinner towards the deep
252 basin.
253 The second seismic facies observed within or at the base of slope consists of composite facies
254 such as chaotic to discontinuous seismic facies packages, bright steeply-dipping reflections,
255 rotated discontinuous stratal re-flections and low amplitude structureless facies (Figure 6).
256 Each of these facies can be interpreted as mass transport deposits/complexes (MTD/MTC)
257 with its headscarp and toe (*e.g.* Bull et al., 2009). The mass-transport complexes (MTC) are
258 the result from the destabilization of sedimentary material by gravitational processes. Most of
259 the observed MTCs in this study area show on seismic sections an elongated geometry with
260 chaotic and discontinuous reflections of variable amplitude (Figure 6). The base and top of the
261 MTCs are often associated with a high amplitude continuous seismic reflection that is better
262 imaged in the downslope parts of the basin and gradually onlaps the slope (Figure 6A). The
263 MTCs within the study area have thicknesses ranging between 50 and 1000 m over an average
264 length of 70 km.

265 *3.2.3. Sediment remobilization by bottom-water currents from the Albian to the Late*
266 *Cretaceous*

267 Sedimentary features related to bottom-water currents have been observed both within the
268 Albian-Cenomanian interval and in the Upper Cretaceous (Figures 6B and 7). The oldest
269 structures are particularly observed at the base of the slope of the Guinean Plateau (Figures
270 4C and 6B). Albian sediment waves are characterized by draping continuous reflections of
271 variable amplitudes leading to characteristic wavy structures (Figure 6B). Their average

length is about 2 km and their average thickness is 200 m. These sediment waves migrate upslope towards the east, as expressed by displacement of their crests (Figure 6B) and are not associated to any turbiditic fan in this interval. On top of this deposit, elongated-mounded contourite drifts accumulated during the Cenomanian, shown as continuous low amplitude reflections with mounded geometry. These reflection packages are bounded by non–depositional zones, the moats, which are revealed by particular reflection terminations (*e.g.* toplaps and onlaps, Figure 6B). These contourite drifts have an average thickness of 200 m and their length varies between 5 and 15 km.

Other examples of sedimentary features related to ocean bottom-water currents have been observed within the Upper Cretaceous in the Senegal and Mauritania basins (Figures 3C, 4A and 7). Numerous sediment waves with an average wavelength of 3 km and a thickness of 100 to 200 m were deposited in the proximal part of the Senegal deep-water basin seismic profile and the DSDP Site 367 (Figure 7A). Some of them are coeval with the deposition of the MTC and show crest migration upslope towards the east (Figure 7A). In southern Mauritania, several elongated mounded structures have been identified that indicate the action of bottom-water currents (Figure 7B). These are associated with low angle incisions on their flank, which represent the moat where bottom-currents flow faster and mobilize sediment on the flank to build a contourite drift. No canyon or indication of downslope transport has been identified in trend with this moat. The moats are characterized by low to moderate continuous reflections which present terminations in downlap and toplap (Figure 7B). The mound crests migrate southward (upslope). These contourite drifts are similar to those observed in Guinea within the Cenomanian section, where they have an average length of 5 to 15 km and a thickness ranging between 200 and 300 m (Figure 6B).

3.3. Cretaceous palaeobathymetry of slope and deep–water basin domains

296 Flexural 2D backstripping of four seismic profiles illustrates the geometry of the margin in
297 Senegal, Mauritania and Guinea (Figures 3 and 4) and allows us to quantify the paleo water-
298 depth in which the sedimentary features, generated by gravity process or ocean bottom current
299 activity, were deposited. The result along the E–W Mauritania profile (Figures 4A and 8A)
300 shows that the unloaded sediments at 93 Ma (top Cenomanian) were deposited at a maximum
301 paleo–depth ranging between 3800 m (T_e = 0 Km) and 3750 m (T_e = 30 km) while at 100 Ma
302 (top Albian), the maximum palaeobathymetry in the basin ranged from 4150 m (T_e = 0 km) to
303 4000 m (T_e = 30 km). Along the N–S Mauritania section (Figure 4A), contourite drifts (Figure
304 7B) are identified and interpreted as 100 Ma old from 2600 m (T_e= 0 km) to 2200 m depth
305 (T_e= 30 km) and at 93 Ma between 2550 m (T_e= 0 km) and 2300 m (T_e = 30 km, Figure 8B).
306 In the Senegal Basin where sedimentary bodies related to bottom–water current were
307 deposited during the Lower Cretaceous (Figure 5), the maximum of the estimated
308 palaeobathymetry ranges from 5550 m (T_e = 0 km) to 5700 m (T_e = 30 km) at 145 Ma (base of
309 the sheeted contourite drift, Figure 8C). At 125 Ma (top of the sheeted contourite drift), the
310 water depths are estimated to reach 5300 m (T_e = 0 km) or 5400 m (T_e = 30km, Figure 8C).
311 The sediment waves observed on this profile (Figure 7A) were deposited after 93 Ma at a
312 depth ranging from 5150 m (T_e = 0 km) to 5050 m (T_e = 30km, Figure 8C). The sediment
313 waves observed offshore Guinea during the Albian (Figure 6B) were formed in a water depth
314 ranging between 4200 m (T_e = 0 km) and 4100 m (T_e = 30 km, Figure 8D). During the
315 Cenomanian, the estimated paleo–depth of the contourite drift (Figure 6B) ranges from 4150
316 m (T_e = 0 km) to 4050 m (T_e = 30 km, Figure 8D).

317 **4. Discussion**

318 4.1. Evolution of the Cretaceous deep-water sedimentation

319 The margin geometry between Mauritania, Senegal and Guinea shows some differences
320 during the Cretaceous (Figures 3 and 4), which may influence sedimentation in the deep-

water basin. Indeed, two types of sedimentary features have been observed: (1) those related to gravitational processes, including channel-levee complexes and mass transport complexes and (2) those related to the remobilization of sediments, either in suspension or from the seafloor, by oceanic bottom currents, including contourite drifts and sediment waves.

Based on the results of our study, a three-stage evolution of Cretaceous deep-water sedimentation is defined (Figure 9). Three paleogeographic maps illustrating the evolution of sedimentation in the eastern Central Atlantic depict geological time intervals of the Lower Cretaceous (Neocomian to Albian, Figure 9A), the Albian-Cenomanian (Figure 9B) and the Upper Cretaceous (from the Turonian to the Maastrichtian, Figure 9C).

4.1.1. Initiation of distal bottom currents during the Lower Cretaceous

During the Lower Cretaceous, few deep-sea fans formed along the slope and remained mostly located off Senegal (Figure 9A). This finding suggests that basin sedimentation (from the base of the slope) was mainly influenced by turbidity currents. In addition, at DSDP Site 367 seismic interpretation and cored sediments show argillaceous and carbonate facies deposited in deep pelagic environments during the Lower Cretaceous (Aptian excluded), occasionally influenced by turbidity currents (Jansa et al., 1978). The Lower Cretaceous unit thickens towards the west, which is inconsistent with turbidity current-driven sedimentation and presents morphological characteristics similar to abyssal sheeted drifts (Faugères et al., 1999; Rebesco et al., 2014). Such bodies are also observed in the Namibian basin and off the NW Iberian Margin during the Cretaceous (Hopkins, 2006, Soares et al., 2014). We suggest that these deposits mark the presence of a bottom current driving remobilization and deposition of sediments near the location of DSDP Site 367. This bottom current would have developed at a water-depth of almost 4000 m, as indicated by the backstripped section (Figure 8C). In the lower part of the Lower Cretaceous limestone sampled at DSDP Site 367, the 'filament microfacies' has been interpreted as an indicator of sediment reworking by bottom currents

346 (Jansa et al., 1978) consistent with the sheeted contourite drift observed in the vicinity of
347 DSDP Site 367 (Figure 5B). In addition, the upper section drilled at this site shows
348 remobilized turbidites (Jansa et al., 1978).

349 *4.1.2. Evidence of Albian to Cenomanian bottom currents within a gravity-driven deep*
350 *sedimentation setting*

351 From the Albian to the end of the Cenomanian, sedimentation in the basin of the eastern
352 Central Atlantic Ocean was mostly influenced by gravity-driven processes, particularly by
353 turbidity currents. This influence is illustrated by regular and continuous deposition of deep-
354 sea fans exclusively located along the base of the continental slope (Figure 9B). In
355 comparison with the Lower Cretaceous, increasing number of deep-sea fan deposits illustrates
356 an increase in the sedimentary material exported to the basin from the continent. This change
357 in sedimentation is also evidenced by the sequence at DSDP Site 367 with Jurassic
358 sedimentation predominantly pelagic and carbonate-rich but becoming detrital-dominated in
359 the Lower Cretaceous (Lancelot et al., 1978a). This change is related to higher sedimentary
360 inputs by several deltas along the Northwest African coast since the Albian (Flicoteaux et al.,
361 1988; Davison et al. 2005; Figure 9B).

362 Increasing detrital contribution preserved at DSDP 367 is associated with turbidity currents
363 supply to the basin with sediments that originated from the river mouth (Jansa et al., 1978).
364 However, erosion surfaces and sharp contacts observed in the Albian-Cenomanian black shale
365 sequence could also be related to remobilization processes. Indeed, it has been shown that
366 sedimentation on most modern margins is influenced by the combined action of gravity-
367 driven processes and bottom current related processes (Faugères et al., 1999; Calvès et al.,
368 2013; Rebesco et al., 2017). In addition, our results clearly show the presence of contourite
369 drifts and sediment wave fields related to bottom currents in the southern part of the NW
370 African margin (Figures 6B and 9B). This observation indicates that bottom-water currents

371 remobilized deep sea sediments in the Albian-Cenomanian offshore southern Senegal and
372 downslope on the Guinean Plateau (Figure 9B). These contour-current sedimentary features
373 are observed to have formed further offshore than the depositional zone dominated by
374 turbidity currents. Such bodies are coeval with deep-sea fan deposition, this indicates that the
375 NW African Margin was influenced by mixed sedimentation in the basin since the Albian.
376 This observation is consistent with prior work by Wynn et al. (2000), who demonstrated that
377 the modern NW African margin is influenced by both gravity-driven and bottom current
378 related processes (Figure 1) in similar bathymetry to that reconstructed for the Albian-
379 Cenomanian period, at 1500 and over 4000 m of water-depth (Figure 8).

380 *4.1.3. Abrupt changes in the Upper Cretaceous deep-sea sedimentation influenced by*
381 *bottom currents*

382 Following the transgression of the early Turonian (~94 Ma), the formation of deep-sea fans in
383 the deep basin ceased and several MTCs formed along the NW African margin (Figure 9C).
384 MTCs are initiated by a loss of stability and then a destabilization of the sediments (Dott,
385 1963). This destabilization may be due, among others, to a vertical movement of the margin
386 that caused sediments to fail, or to excessive sediment accumulation along the continental
387 slope that caused instability and gravitational collapse of the underlying sedimentary cover. In
388 the case of the NW African margin, several geodynamic events such as convergence between
389 Africa and Europe were responsible for deformation and vertical movement in the northern
390 margin (Guiraud and Bosworth, 1997). These forces could be appropriate triggers for MTCs.
391 Indeed, during the Upper Cretaceous, many sediment waves that are laterally associated with
392 MTCs were formed off Senegal in >4000 m water–depth, from the northern Guinean Plateau
393 to the south of Mauritania (Figure 9C). In comparison with the sediment waves deposited
394 during the Albian, these are of greater wavelength and have an extent to the west into the deep
395 basin (Figure 9C). In addition, a contourite drift is located down the continental slope below

1700 m water depth in southern Mauritania is associated with a sediment wave field (Figure 9C). These various elements illustrate the presence of bottom–water currents that appear to have had a stronger influence in Upper Cretaceous deep–water sedimentation compared to earlier since they are observed in greater number (Figure 9).

4.2. Implications for Cretaceous oceanic paleocirculation pattern

Many studies agree on the nature of oceanic circulation patterns in the Central Atlantic Ocean during the Cretaceous. Indeed, it seems that the transition between the Cenomanian and the Turonian (~94 Ma) was a key period illustrating ocean circulation change between the Lower and Upper Cretaceous (Bralower and Thierstein, 1984; Poulsen et al., 2001; Pucéat et al., 2005; Trabucho Alexandre et al., 2010; Donnadieu et al., 2016). During the Lower Cretaceous, the Atlantic Ocean would have had a slow to sluggish oceanic circulation with very little renewal of water deeper than 1500 m (Barron, 1983; Bralower and Thierstein, 1984). This sluggish circulation would have favoured the development of anoxic and oxygen-depleted waters (Schlanger and Jenkyns, 1976; Bralower and Thierstein, 1984). As a result, an important stratification of the ocean water column is inferred with little or no renewal of deep-water masses (Schlanger and Jenkyns, 1976; Bralower and Thierstein, 1984). The water mass circulation in the Central Atlantic Ocean during the Lower Cretaceous would have exclusively affected water-depths shallower than 500 m, with ocean currents originating from the Tethys Ocean and circulating into the eastern Central Atlantic Ocean (Poulsen et al., 2001; Pucéat et al., 2005). In contrast, palaeogeographic changes during the Turonian, 90–94 Ma (*e.g.,* opening of the Equatorial Atlantic Ocean) would have progressively led to increasing oceanic circulation and better ventilation of the seafloor by bottom currents during the Upper Cretaceous in the whole Central Atlantic (Poulsen et al., 2001; Donnadieu et al., 2016). This change would have resulted in the formation of deep-water currents that originated from the eastern Pacific and the South Atlantic oceans, and flowed northward to the Central Atlantic

421 Ocean (Poulsen et al., 2001; Trabucho Alexandre et al., 2010; Robinson and Vance, 2012;
422 Voigt et al., 2013; Donnadieu et al., 2016). Our results show an evolution of deep-sea
423 sedimentation with a similar timing to that currently proposed for the evolution of the
424 palaeocirculation of the Central Atlantic Ocean during the Cretaceous. Indeed, we observe
425 more sedimentary features related to bottom currents in the Upper Cretaceous sequence than
426 during the preceding Mesozoic periods (Figures 9 and 10). In addition, this study confirms the
427 presence of bottom currents during the Upper Cretaceous as proposed by Robinson and Vance
428 (2012) and constrains the palaeobathymetry at which these bottom currents affected the
429 sedimentation (Figures 8). These constraints help to reduce the great uncertainty about
430 Cretaceous palaeobathymetry in the eastern Central Atlantic Ocean. Actually, the paleowater–
431 depths of the Cretaceous bottom currents had been estimated by modeling and by neodymium
432 isotope analysis in fish teeth, but it remained qualitative (Poulsen et al., 2001; MacLeod et al.,
433 2008; Trabucho Alexandre et al., 2010; Donnadieu et al., 2016). It is now clear that the
434 Central Atlantic Ocean palaeobathymetry was already close to present-day depth since the
435 Lower Cretaceous (>4000 m in the deep basin, Figure 8C). Moreover, the organization of the
436 modern water column on the NW African margin involves surface (0-~600 m), intermediate
437 (~600-1500 m) and the deep-waters that extend down to 4000 m depth with specific
438 temperatures and salinities (Figure 10A). These water masses originate from other basins,
439 including the South Atlantic and the Antarctic Oceans (Emery and Meincke, 1986).
440 Bathymetry and water column stratification of the eastern Central Atlantic Ocean could be
441 similar between the Upper Cretaceous and present-day, which is consistent with the
442 establishment of a global circulation since the Upper Cretaceous (Poulsen et al., 2001).

443 However, our results do not support the hypothesis that proposes a sluggish to slow deep–
444 water circulation for the Central Atlantic Ocean before the Upper Cretaceous (Barron, 1983;
445 Bralower and Theirstein, 1984, Poulsen et al., 2001). Indeed, this work documents the

446 presence of active bottom currents flowing since the Lower Cretaceous (Figures 5, 6, 9 and
447 10) which suggests active deep oceanic circulation since the Early Cretaceous. This findings
448 supported by other studies which have illustrated the movements of deep-water masses
449 flowing in the Central Atlantic Ocean during the Cretaceous. For example, Soares et al.
450 (2014) in a study of the northwest of the Iberia margin and in a study of Dunlap et al. (2013)
451 offshore Morocco illustrated the presence of contourite drifts and sediment waves on the
452 seafloor since the Lower Cretaceous. Dunlap et al. (2013) proposed that sediment waves
453 evolved in water-depths of <3000 m, which is similar to water depths for sediment waves and
454 contourite drift development observed in this study offshore of Mauritania and Guinea
455 (Figures 8B and 10B).

456 **5. Conclusions**

457 This study provides evidence of sedimentary features related to bottom current activity and
458 layered oceanic circulation since the Lower Cretaceous in the Central Atlantic offshore of
459 Mauritania and Guinea. Lower Cretaceous contourite drifts formed in paleowater-depths of
460 >4000 m in the distal domain of the NW African margin near the location of DSDP Site 317.
461 During the Albian-Cenomanian, contourite drifts and sediment waves formed along the base
462 of the continental slope and combined with gravity-driven sedimentation in the Guinean and
463 Senegal basins. From the Turonian to the Maastrichtian, an increase in the number of
464 sediment wave fields is noted in the abyssal plain of the Senegal Basin. These particular
465 features seem disconnected from gravity-driven sedimentation that affected the slope and the
466 proximal parts of the abyssal plain. In addition, contourite drifts were identified in the
467 Mauritanian basin during this period. These results support an Upper Cretaceous oceanic
468 model of a better ventilated Central Atlantic Ocean, and bottom current flow starting in the
469 Lower Cretaceous which is inconsistent with hypotheses that call for a sluggish to stagnant
470 ocean at that time. Heterogeneity of sediments associated with organic rich sediments in the

eastern Central Atlantic domain has been unraveled by tracing methods (Mourlot et al., 2018). More works of the Cretaceous deep-sea sediments and oceans circulation still need to be done.

AUTHORS CONTRIBUTIONS

Y.M. and G.C. designed the study and implemented the analysis. Y.M. G.C. P.D.C. G.B. A.-C.C. and F.R. contributed to data analysis. F.R. and A.-C.C. supported Y.M. for data handling and in-house management. The manuscript was written by G.C. and Y.M.

ACKNOWLEDGMENTS

Y.M. and G.B. thank Total E&P for funding their research project at the Université Toulouse 3 – Paul Sabatier. Thanks to François Leparmentier, Jean-Marc Pince (Total E&P) and Samuel Toucanne (IFREMER, LGS, Plouzané) for valuable discussions. We also thank Alan Roberts and Nick Kusznir for allowing us to use Flex–Decomp™. We are grateful to TGS for the permission to publish the seismic lines. Seismic data sourced from the Virtual Seismic Atlas (VSA; link) have been used to produce the Figure 3A (survey: VER-01 MWT and VERMAU-01, seismic data property of CGG Veritas). PC thanks the Charles T. McCord Jr Chair in Petroleum Geology at LSU. We would also like to thank the editor Jean-Philippe Avouac, Joe Cartwright and an anonymous reviewer for their helpful comments.

REFERENCES

Barron, E. J., 1983. A warm, equable Cretaceous: The nature of the problem, Earth Sci. Rev., 19, 305–338

Berrocoso, A.J., MacLeod, K.G., Martin, E., Bourbon, E., Londoño, C.I., and Basak, C., 2010. Nutrient trap for Late Cretaceous organic–rich black shales in the tropical North Atlantic: Geology, v. 38, p. 1111–1114. doi:10.1130/G31195.1.

494 Boyer, T.P., J. I. Antonov, O. K. Baranova, C. Coleman, H. E. Garcia, A. Grodsky, D. R.
495 Johnson, R. A. Locarnini, A. V. Mishonov, T.D. O'Brien, C.R. Paver, J.R. Reagan, D. Seidov,
496 I. V. Smolyar, and M. M. Zweng, 2013. World Ocean Database 2013, NOAA Atlas NESDIS
497 72, S. Levitus, Ed., A. Mishonov, Technical Ed.; Silver Spring, MD, 209 pp.,
498 doi:10.7289/V5NZ85MT

499 Bralower, T. J., and Thierstein, H. R., 1984. Low productivity and slow deep–water
500 circulation in mid–Cretaceous oceans. Geology, 12(10), 614–618.

501 Bull, S., Cartwright, J., and Huuse, M., 2009. A review of kinematic indicators from mass-
502 transport complexes using 3D seismic data. Marine and Petroleum Geology, 26(7), 1132–
503 1151. https://doi.org/https://doi.org/10.1016/j.marpetgeo.2008.09.011

504 Calvès, G., Clift, P. D., and Inam, A., 2008. Anomalous subsidence on the rifted volcanic
505 margin of Pakistan: No influence from Deccan plume. Earth and Planetary Science Letters,
506 272(1–2). doi:10.1016/j.epsl.2008.04.042

507 Calvès, G. , Toucanne, S. , Jouet, G. , Charrier, S. , Thereau, E. , Etoubleau, J. , Marsset, T. ,
508 Droz, L. , Bez, M. , Abreu, V. , Jorry, S. , Mulder, T. and Lericolais, G., 2013, Inferring
509 denudation variations from the sediment record; an example of the last glacial cycle record of
510 the Golo Basin and watershed, East Corsica, western Mediterranean sea. Basin Res, 25: 197-
511 218. doi:10.1111/j.1365-2117.2012.00556.x

512 Clift, P. D., Turner, J., and Party, T. O. D. P. L. 152 S., 1995. Dynamic support by the Iceland
513 Plume and its effect on the subsidence of the northern Atlantic margins. Journal of the
514 Geological Society, 152(6), 935–941. doi:10.1144/GSL.JGS.1995.152.01.09

515 Davison, I., 2005. Central Atlantic margin of North West Africa: Geology and hydrocarbon
516 potential (Morocco to Guinea), J. Afr. Earth Sci., 43, 254–274,
517 doi:10.1016/j.jafrearsci.2005.07.018.

518 Donnadieu, Y., Pucéat, E., Moiroud, M., Guillocheau, F., Deconinck, J.–F., 2016. A better–
519 ventilated ocean triggered by Late Cretaceous changes in continental configuration. Nature
520 Communications 7, 10316. doi:10.1038/ncomms10316

521 Dott, R.H., 1963. Dynamics of subaqueous gravity depositional processes. AAPG Bull.,
522 47,104–128.

523 Dunlap, D., Wood, L., Moscardelli, L., 2013. Seismic geomorphology of early North Atlantic
524 sediment waves, offshore northwest Africa. Interpretation 1, SA75–SA91. doi:10.1190/INT–
525 2013–0040.1

526 Emery, K. O., and Uchupi, E,. 1984. The geology of the Atlantic Ocean. Springer Science &
527 Business Media. doi: 10.4319/lo.1986.31.3.0669

528 Emery, W.J., and Meincke J., 1986. Global water masses: Summary and review, Oceanologia
529 Acta, 9(4), 383–391.

530 Faugères, J.–C., Stow, D.A.V., Imbert, P., Viana, A., 1999. Seismic features diagnostic of
531 contourite drifts. Marine Geology 162, 1–38. doi:10.1016/S0025–3227(99)00068–7

532 Flicoteaux, R., Latil–Brun, M.–V., Michaud, L., 1988. Histoire de la subsidence post–rift du
533 bassin côtier mauritano–sénégalo–guinéen. Relation avec l'amincissement crustal pendant la
534 période jurassique à Crétacé inférieur. Comparaison avec l'évolution des marges péri–
535 atlantiques au niveau de l'Atlantique Central et Equatorial (côte est des U.S.A., Sud–Sahara,
536 Côte d'Ivoire et Plateau du Demerara). Journal of African Earth Sciences (and the Middle

East), The West African connection: Evolution of the central atlantic ocean and its Continental Margins 7, 345–359. doi:10.1016/0899–5362(88)90079–6

Flood, R. D., Manley, P. L., Kowsmann, R. O., Appi, C. J., Pirmez, C., 1991. Seismic Facies and Late Quaternary Growth of Amazon Submarine Fan BT - Seismic Facies and Sedimentary Processes of Submarine Fans and Turbidite Systems. In P. Weimer & M. H. Link (Eds.) (pp. 415–433). New York, NY: Springer New York. doi:10.1007/978-1-4684-8276-8_23

Guiraud, R., Bosworth, W., 1997. Senonian basin inversion and rejuvenation of rifting in Africa and Arabia: synthesis and implications to plate–scale tectonics. Tectonophysics, Structural Controls on Sedimentary Basin Formation 282, 39–82. doi:10.1016/S0040–1951(97)00212–6

Hardenbol, J., Vail, P. R., Ferrer, J., Montadert, L., and Blanchet, R., 1981. Interpreting paleoenvironments, subsidence history and sea–level changes of passive margins from seismic and biostratigraphy. Oceanologica Acta, Special issue, 2, 33–44.

Heezen, B.C., Hollister, C., 1964. Deep–sea current evidence from abyssal sediments. Marine Geology 1, 141–174. doi:10.1016/0025–3227(64)90012–X

Hernández-Molina, F. J., Maldonado, A., & Stow, D. A. V. 2008a. Chapter 18 Abyssal Plain Contourites. Developments in Sedimentology, 60, 345–378. doi:10.1016/S0070-4571(08)10018-8

Hernández–Molina F.J., Llave E., Stow D.A.V., 2008b. Chapter 19 Continental Slope Contourites, Developments in Sedimentology, 60, 379–408. doi:10.1016/S0070–4571(08)10019–X

559 Hopkins, A.E., 2006. Seismic stratigraphic interpretation of contourite systems, Namibian
560 continental margin. PhD Thesis, University of Cardiff, Cardiff.

561 Jansa, L., Gardner, J.V., Dean, W.E., 1978. Mesozoic sequences of the Central North
562 Atlantic. Initial Reports of the Deep Sea Drilling Project. doi:10.2973/dsdp.proc.41.138.1978

563 Kusznir, N. J., Roberts, A. M., and Morley, C. K., 1995. Forward and reverse modelling of
564 rift basin formation. Geological Society, London, Special Publications, 80(1), 33–56. doi:
565 10.1144/GSL.SP.1995.080.01.02

566 Lancelot, Y., Seibold, E., Cepek, P., Dean, W.E., Eremeev, V., Gardner, J.V., Jansa, L.,
567 Johnson, D., Kasheninnikov, V., Pflaumann, U., Graham, J., Bukry, D., 1978a. Site 367: Cape
568 Verde Basin. Initial Reports of the Deep Sea Drilling Project 41, 163–232.
569 doi:10.2973/dsdp.proc.41.103.1978

570 Lancelot, Y., Seibold, E., Cepek, P., Dean, W.E., Eremeev, V., Gardner, J.V., Jansa, L.,
571 Johnson, D., Kasheninnikov, V., Pflaumann, U., Graham, J., Bukry, D., 1978b. Site 368:
572 Cape Verde Rise. Initial Reports of the Deep Sea Drilling Project 41, 233–326.
573 doi:10.2973/dsdp.proc.41.104.1978

574 Latil–Brun, M.V. and Lucazeau, F., 1988. Subsidence, extension and thermal history of the
575 West African margin in Senegal. Earth and Planetary Science Letters, 90(2): 204–220. doi:
576 10.1016/0012–821X(88)90101–X

577 Labails, C., 2007. La marge sud–marocaine et les premières phases d'ouverture de l'océan
578 Atlantique Central. PhD Thesis. Université de Bretagne Occidentale).

579 MacLeod, K.G., Martin, E.E., Blair, S.W., 2008. Nd isotopic excursion across Cretaceous
580 ocean anoxic event 2 (Cenomanian–Turonian) in the tropical North Atlantic. Geology 36,
581 811–814. doi:10.1130/G24999A.1

582 Martin, E.E., MacLeod, K.G., Jiménez Berrocoso, A., Bourbon, E., 2012. Water mass
583 circulation on Demerara Rise during the Late Cretaceous based on Nd isotopes. Earth and
584 Planetary Science Letters 327–328, 111–120. doi:10.1016/j.epsl.2012.01.037

585 Mosher, D. C., Campbell, D. C., Gardner, J. V, Piper, D. J. W., Chaytor, J. D., and Rebesco,
586 M., 2017. The role of deep-water sedimentary processes in shaping a continental margin: The
587 Northwest Atlantic. Marine Geology, 393, 245–259. doi:10.1016/j.margeo.2017.08.018

588 Mourlot, Y., Roddaz, M., Dera, G. Calvès, G., Kim, J.H., Chaboureau, A-C., Mounic, S., and
589 Raison, F., 2018, Geochemical evidence for large-scale drainage reorganization in Northwest
590 Africa during the Cretaceous, G-Cubed, doi:10.1029/2018GC007448

591 Mullins H.T., and Neumann, A.C., 1979. Deep carbonate bank–margin structure and
592 sedimentation in the northern Bahamas. SEPM Publ., 27, 165–192.

593 Patriat, M., and Labails, C., 2006. Linking the Canary and Cape–Verde hot–spots, northwest
594 Africa. Marine Geophysical Research, 27(3), 201–215. doi: 10.1007/s11001–006–9000–7

595 Posamentier, H. W., and V. Kolla, 2003. Seismic geomorphology and stratigraphy of
596 depositional elements in deep-water settings, J. Sediment. Res., 73(3), 367– 388.
597 Poulsen, C. J., Barron E. J., Arthur M. A., and Peterson W. H., 2001. Response of the Mid–
598 Cretaceous global oceanic circulation to tectonic and CO2 forcings, Palaeoceanography,
599 16(6), 576–592, doi:10.1029/2000PA000579.

600 Pucéat, E., Lécuyer, C., Reisberg, L., 2005. Neodymium isotope evolution of NW Tethyan
601 upper ocean waters throughout the Cretaceous. Earth and Planetary Science Letters 236, 705–
602 720. doi:10.1016/j.epsl.2005.03.015

603 Purdy, E.G. 1989. Africa Geology and Hydrocarbons Map. Exploration of Africa Project.

Rebesco, M., Hernández–Molina, F.J., Van Rooij, D., Wåhlin, A., 2014. Contourites and associated sediments controlled by deep–water circulation processes: State–of–the–art and future considerations. Marine Geology, 50th Anniversary Special Issue 352, 111–154. doi:10.1016/j.margeo.2014.03.011

Rebesco, M., Mosher, D., & Piper, D. J. W. 2017. Advancements in Understanding Deep-Sea Clastic Sedimentation Processes: a preface. Marine Geology, 393, 1–3. doi:10.1016/j.margeo.2017.10.007

Roberts, A. M., Kusznir, N. J., Yielding, G., & Styles, P., 1998. 2D flexural backstripping of extensional basins: the need for a sideways glance. Petroleum Geoscience, 4(4), 327-338.

Roberts, A. M., R. I. Corfield, N. J. Kusznir, S. J. Matthews, E.–Kåre Hansen, and R. J. Hooper 2009. Mapping palaeostructure and palaeobathymetry along the Norwegian Atlantic continental margin: Møre and Vøring basins, Petroleum Geoscience, 15(1), 27–43, doi:10.1144/1354–079309–804

Robinson, S.A., Vance, D., 2012. Widespread and synchronous change in deep–ocean circulation in the North and South Atlantic during the Late Cretaceous. Palaeoceanography 27, PA1102. doi:10.1029/2011PA002240

Ryan, W.B.F., Sibuet, J–C., Arthur, M.A., Lopatin, B.G., Moore, D.G., Maldonado, A., Rehault, J–P., Iaccarino, S., Sigal, J., Morgan, G.E., Blechschmidt, G., Williams, A.C., Johnson, D., Barnes, R.O., and Habib, D., 1979. 2. Site 398. Initial Reports of the Deep Sea Drilling Project 47B, 25–233. doi:10.2973/dsdp.proc.47–2.102.1979

Schlanger, S. O., and Jenkyns, H. C., 1976. Cretaceous oceanic anoxic events: causes and consequences. Geologie en mijnbouw, 55(3–4), 179–184.

626 Schwab, A.M., Tremblay, S., Hurst, A., 2007. Seismic expression of turbidity–current and
627 bottom–current processes on the Northern Mauritanian continental slope. Geological Society,
628 London, Special Publications 277, 237–252. doi:10.1144/GSL.SP.2007.277.01.14

629 Shipboard Scientific Party and David Bukry, 1978. Site 367: Cape Verde Basin, Part II: Site
630 Reports, in: DSDP Volume 41 (ed. Lancelot et al.), 163–232,
631 doi:10.2973/dsdp.proc.41.103.1978

632 Soares, D.M., Alves, T.M., Terrinha, P., 2014. Contourite drifts on early passive margins as
633 an indicator of established lithospheric breakup. Earth and Planetary Science Letters 401,
634 116–131. doi:10.1016/j.epsl.2014.06.001

635 Stow, D. a. V., Pudsey, C.J., Howe, J.A., Faugères, J.–C., Viana, A.R., 2002. Deep–water
636 contourite systems: Modern drifts and ancient series, seismic and sedimentary characteristics.
637 Geological Society Memoir.

638 Trabucho Alexandre, J., Tuenter, E., Henstra, G. A., van der Zwan, K. J., van de Wal, R. S.,
639 Dijkstra, H. A., and de Boer, P. L., 2010. The mid-Cretaceous North Atlantic nutrient trap:
640 Black shales and OAEs. Palaeoceanography, 25(4). doi: 10.1029/2010PA001925

641 Uenzelmann–Neben, G., Weber, T., Grützner, J., Thomas, M., 2016. Transition from the
642 Cretaceous ocean to Cenozoic circulation in the western South Atlantic — A twofold
643 reconstruction. Tectonophysics. doi:10.1016/j.tecto.2016.05.036

644 Voigt, S., Jung, C., Friedrich, O., Frank, M., Teschner, C., Hoffmann, J., 2013. Tectonically
645 restricted deep–ocean circulation at the end of the Cretaceous greenhouse. Earth and Planetary
646 Science Letters 369–370, 169–177. doi:10.1016/j.epsl.2013.03.019

647 von Rad, U, and Einsele, G., 1980. The evolution of passive continental margins in the light
648 of recent deep drilling results – Mesozoic–Cainozoic subsidence history and

649 palaeobathymetry of the northwest African continental margin (Aaiun Basin to D. S. D. P.
650 Site 397). Philosophical Transactions of the Royal Society of London. Series A, Mathematical
651 and Physical Sciences, 294(1409), 37 LP–50.

652 von Rad, U., Hinz, K., Sarnthein, M. and Seibold, E. 1982. (Eds.), Geology of the Northwest
653 African Continental Margin, 107–131, 12 figs., Berlin, Heidel–berg, New York (Springer).

654 Watts, A. B., 1978. An analysis of isostasy in the world's oceans 1. Hawaiian–Emperor
655 Seamount Chain, J. Geophys. Res., 83(B12), 5989–6004, doi:10.1029/JB083iB12p05989.

656 Watts, A. B., 2015. 6.01 – Crustal and Lithosphere Dynamics: An Introduction and Overview
657 A2 – Schubert, Gerald BT – Treatise on Geophysics (Second Edition) (pp. 1–44). Oxford:
658 Elsevier, doi:10.1016/B978–0–444–53802–4.00110–X

659 Wynn, R.B., Weaver, P.P.E., Ercilla, G., Stow, D.A.V., Masson, D.G., 2000. Sedimentary
660 processes in the Selvage sediment–wave field, NE Atlantic: new insights into the formation of
661 sediment waves by turbidity currents. Sedimentology 47, 1181–1197. doi:10.1046/j.1365–
662 3091.2000.00348.x

663

TABLE

Section	Figure	Stratigraphic interval	Age (Ma)	Porosity (%)	Density (g/cc)	Lithology			
						% Sand	% Silty clay	% Shale	% [illegible]
Mauritania Basin	5A	Base Cenozoic to present-day seafloor	65 to 0	52.5	2.50	45	10	25	32
		Top Cenomanian to base Cenozoic	93 to 65	33.5	2.33	32	10	22	30
		Top Albian to top Cenomanian	100 to 93	44.1	2.58	40	0	20	40
		Top Lower Cretaceous to top Albian	125 to 100	33.5	2.33	30	22	0	12
		Top Jurassic to top Lower Cretaceous	145 to 125	[illegible]	2.57	40	25	0	35
		Top Acoustic Basement to top Jurassic	170 to 145	21.0	2.7	0	0	10	50
Senegal Basin	5B	Base Cenozoic to present-day seafloor	65 to 0	55.5	2.21	50	0	15	15
		Top Cenomanian to base Cenozoic	93 to 65	32.5	2.29	45	0	40	15
		Top Albian to top Cenomanian	100 to 93	55.8	2.20	18	0	25	64
		Top Aptian to top Albian	113 to 100	24.6	2.29	12	0	35	52
		Top Lower Cretaceous to top Aptian	125 to 113	55.5	2.21	50	0	20	10
		Top Jurassic to top Lower Cretaceous	145 to 125	21.7	2.29	2	25	35	40
		Top Acoustic Basement to top Jurassic	170 to 145	[illegible]	2.71	[illegible]	0	10	50
Mauritania Basin	4A	Base Cenozoic to present-day seafloor	65 to 0	33.5	2.33	40	10	15	32
		Top Cenomanian to base Cenozoic	93 to 65	44.5	2.53	32	18	22	40
		Top Albian to top Cenomanian	100 to 93	55.3	2.56	50	0	20	50
		Top Aptian to top Albian	113 to 100	33.5	2.33	45	52	0	5
		Top Lower Cretaceous to top Aptian	125 to 113	[illegible]	2.57	40	40	0	40
		Top Jurassic to top Lower Cretaceous	145 to 125	21.0	2.7	0	0	10	50
[illegible]	4B	Base Cenozoic to present-day seafloor	65 to 0	54.0	2.21	50	0	50	40
		Top Cenomanian to base Cenozoic	93 to 65	27.7	2.27	5	0	90	5
		Top Albian to top Cenomanian	100 to 93	54.0	2.22	[illegible]	0	50	10
		Top Aptian to top Albian	113 to 100	33.7	2.33	55	5	35	5
		Top Lower Cretaceous to top Aptian	125 to 113	54.0	2.22	20	0	20	60
		Top Jurassic to top Lower Cretaceous	145 to 125	21.7	2.29	2	25	35	40
		Top Acoustic Basement to top Jurassic	170 to 145	[illegible]	[illegible]	[illegible]	0	10	50

Table 1: Lithology, porosity and density parameters for each sedimentary unit used for the backstripping of stratigraphic cross section illustrated in Figures 3 and 4.

SUPPLEMENTAL FILES

Figure S1: Figure S1: (A) Original map of the Site 367 in the Cape Verde Basin, with location of seismic reflection profiles (Shipboard Scientific Party, 1978). (B) Portion of VEMA 29 seismic profile crossing Site 367, Horizons A, B and C corresponds to targets prior of drilling, (C and D) Portions of seismic profile Valvidia 10, with seismic calibrated framework corresponding to (E.) Figure 5A. SF: Sea Floor; P: Base Paleocene; TC: Top Cenomanian; TA: Top Albian; TAp: Top Aptian; TLC: Top Lower Cretaceous; AB: Top Acoustic Basement.

Figure S2: (A) Time–depth plot of velocity measurements from radiosonobuoys located off Mauritania and Senegal compiled by Diebold (1996) and checkshot data sourced from DSDP Sites 368, 657 and 397 initial reports (Lancelot et al., 1978b; von Rad et al., 1979; Shipboard Scientific Party, 1988). (B) Porosity curves used for decompaction in FlexDecomp (Sclater and Christie, 1980).

Figure S3: (A) Grid map illustrating the repartition of Te data of the continental and oceanic lithospheres sourced by Watts (2015). Delimitation of the continental and the ocean realms is characterized by the Ocean-Continent Boundary (OCB) sourced by Müller et al. (2016). (B) Distribution and frequency of Te values in the continental and ocean realms.

686 **FIGURE CAPTIONS**

687 Figure 1: Shaded bathymetric map of the eastern Central Atlantic Ocean showing the
688 geomorphological and oceanographic framework of the studied margin between the Canary
689 Island Seamount Province (CISP) and the Guinean Plateau (GP). Interaction between oceanic
690 currents and terrestrial sedimentary export is illustrated by four regional seismic sections
691 indicated by red lines through Deep Sea Drilling Project (DSDP) Sites 367 and 368. Grey area
692 represents the basement bulge off the margin identified by Patriat and Labails (2006) and the
693 location of the Jurassic shelf edge mapped by Purdy (1989). Magnetic anomalies are
694 reconstructed by Labails (2007). Cretaceous sediment waves observed by Dunlap et al. (2013)
695 are indicated by the blue star. Present-day sediment wave fields are sourced from Wynn et al.
696 (2000). Present-day oceanic circulation with GS–NAC: Gulf Stream–North Atlantic Current.
697 CC: Canary Current. NEC: North Equatorial Current. ECC: Equatorial Counter–Current.
698 ABW: Antarctic Bottom Water. Cretaceous oceanic currents correspond to the Tethys
699 Circumglobal Current (TCC) proposed by Pucéat et al. (2005), the Demerara Bottom Water
700 (DBW) proposed by Berrocoso et al. (2010), the North Component Waters (NCW) and the
701 Southern Component Waters (SCW) proposed by Robinson and Vance (2012). MSB:
702 Morocco Salt Basin. AB: Aaiun Basin. MSGB: Mauritania Senegal Guinea Basin. SLB:
703 Sierra Leone Basin. SLR: Sierra Leone Rise. Base map sourced from the Geomapapp©
704 (http://www.geomapapp.org/)

705 Figure 2: Lithostratigraphic chart of DSDP Sites 367, 368 (Mauritania Senegal Guinea Basin;
706 Lancelot et al., 1978a; 1978b), DSDP Site 398 (NW Iberian Margin; Ryan et al., 1979) and
707 sedimentary structures identified in this study area. Sediment waves and mass transport
708 complex occurrence offshore Morocco is based on Dunlap et al. (2013) and contourite drift
709 occurrences offshore the NW Iberian Margin is from Soares et al. (2014). Age uncertainties
710 are illustrated by dashed-black arrows. TD: Total Depth; DbF: Debris Flow.

711 Figure 3: (A) East-West two-way time seismic section through DSDP Site 368 (offshore
712 Mauritania), data sourced from the Virtual Seismic Atlas (VSA; link). (B) Interpreted
713 geological depth converted section of Figure 3A. SF: Sea Floor; P: Base Paleocene; TC: Top
714 Cenomanian; TA: Top Albian; TAp: Top Aptian; TLC: Top Lower Cretaceous; AB: Top
715 Acoustic Basement. (C) East-West depth converted seismic section through DSDP Site 367
716 (offshore Senegal), courtesy of TGS. (D) Interpreted geological section of the Figure 3C.
717 Legend is the same as Figure 3B. See Figure 1 for location.

718 Figure 4: (A) North-South two-way time seismic section along the Mauritanian shelf (east of
719 DSDP Site 368, offshore Mauritania), courtesy of TGS. (B) Depth-converted interpreted
720 geological section derived from Figure 4A. (C) WNW-ESE two-way time seismic section
721 through Guinean Plateau to deep-water, courtesy of TGS. (D) Depth converted interpreted
722 geological section derived from Figure 4C. Legend is the same as Figure 3B. See Figure 1 for
723 location.

724 Figure 5: (A) Inset of the W–E regional section across the Senegal Basin (Figure 3C) showing
725 the thickening of the lower Cretaceous sediments on Jurassic deposits observed west of DSDP
726 Site 367 (Courtesy of TGS). (B) Interpreted W–E oriented seismic line flattened along a
727 continuous regional event (Top Aptian: TAp) allowing restoration of the basin geometry at
728 the time of the drowning of the mounded structure associated to sheeted contourite drift.
729 Legend is the same as Figure 3B. See Figure 1 for location.

730 Figure 6: (A) Inset of Cenomanian channel-levee complex deposited at the base of the slope
731 observed on Figure 3C (Courtesy of TGS). High-amplitude reflections: HARs. (B) Inset of
732 Figure 4C illustrating sediment wave and contourite drift deposits between the Albian and
733 Cenomanian intervals. Note the change of scale between the sediment waves and the
734 contourite drift deposits. Mass transport complexes are observed above in the Upper

735 Cretaceous interval. The crest migration of the sediment waves towards the ESE indicates that
736 the deposition of the sediment is controlled by a bottom current coming from the WNW.
737 Legend is the same as Figure 3B. See Figure 1 for location.

738 Figure 7: (A) Inset of Upper Cretaceous sediment waves and mass transport complex
739 observed east of DSDP Site 367 (Senegal) on Figure 3B (Courtesy of TGS). Note the
740 extensive erosional surface at the base of the sediment wave sequence. (B) inset from Figure
741 4A of the offshore Mauritania Basin, the Cenomanian interval is characterized by channel-
742 levee systems whereas the Upper Cretaceous is related to contourite drifts deposits. The crest
743 migration of the contourite drift deposits indicates a sedimentation controlled by a potential
744 oceanic current coming from the North. Legend is the same as Figure 3B. See Figure 1 for
745 location.

746 Figure 8: 2D sediment-unloaded sections along Figures 3 and 4 showing the paleobathymetric
747 evolution of the seafloor during the Cretaceous. Present day seafloor is marked by the
748 continuous black line where as age (Ma)/T_e(km) pairs are associated to different
749 discontinuous lines of different grey scales. Displays are restricted to the areas where bottom
750 current sedimentary features have been observed. (A) E–W Mauritanian section through
751 DSDP Site 368. (B) N–S Mauritanian section. (C) E–W Senegal section through DSDP Site
752 367. (D) WNW–ESE Guinean Basin section.

753 Figure 9: Paleogeographic maps of the study area focused on the deep-water sedimentation.
754 (A) Early Cretaceous period (Berriasian-Aptian), the sedimentation in the deep-water area is
755 associated to channel-levees sourced from onshore via deltas and some sediment waves
756 offshore Morocco and mounded drifts near DSDP Site 367. (B) the Albian-Cenomanian
757 period records extensive slope deposits that covers most of the margins from Morocco to
758 Guinea where contourite drift and upper slope erosion occurs. (C). the Upper Cretaceous

759 period (Turonian to Maastrichtian) is a period of mass slope disturbance with mass transport
760 complexes and important bottom-current sediment wave related fields and contourite drift
761 from Guinea to south Morocco. In the north of the study area a regional hiatus potentially
762 related to uplift/erosion of the margin sourced from the collision of North Africa with
763 European plates.

764 Figure 10: Synthetic present day and Cretaceous oceanographic-seafloor model. (A) Present–
765 day oceanographic properties along the Northwestern African Margin. (B) Cretaceous
766 synthesis of observed sedimentary features occurrences related to bottom–water currents. (C)
767 Evolution of Cretaceous bottom water sedimentary features record. Oceanographic data
768 (temperature, salinity) are sourced from National Oceanic and Atmospheric Administration
769 (NOAA) world ocean database (WOD13, Station 1550019(C): 21°W 14°N) (Boyer et al.,
770 2013). Present–day water masses names and water depths are sourced from Emery and
771 Meincke (1986). SACW: South Atlantic Central Water. ENACW: Eastern North Atlantic
772 Central Water. AIW: Antarctic Intermediate Water. MW: Mediterranean Water. EASIW:
773 Eastern Atlantic Subarctic Intermediate Water. ABW: Antarctic Bottom Waters.
774 Paleobathymetries related to Cretaceous ocean currents are from: DBW – Demerara Bottom
775 Water (Berrocoso et al., 2010); NCW – North Component Waters (MacLeod et al., 2008;
776 Voigt et al., 2013); SCW – South Component Waters (Robinson and Vance, 2012) and TCC –
777 Tethys Circumglobal Current (Pucéat et al., 2005).

Figure 01
Click here to download high resolution image

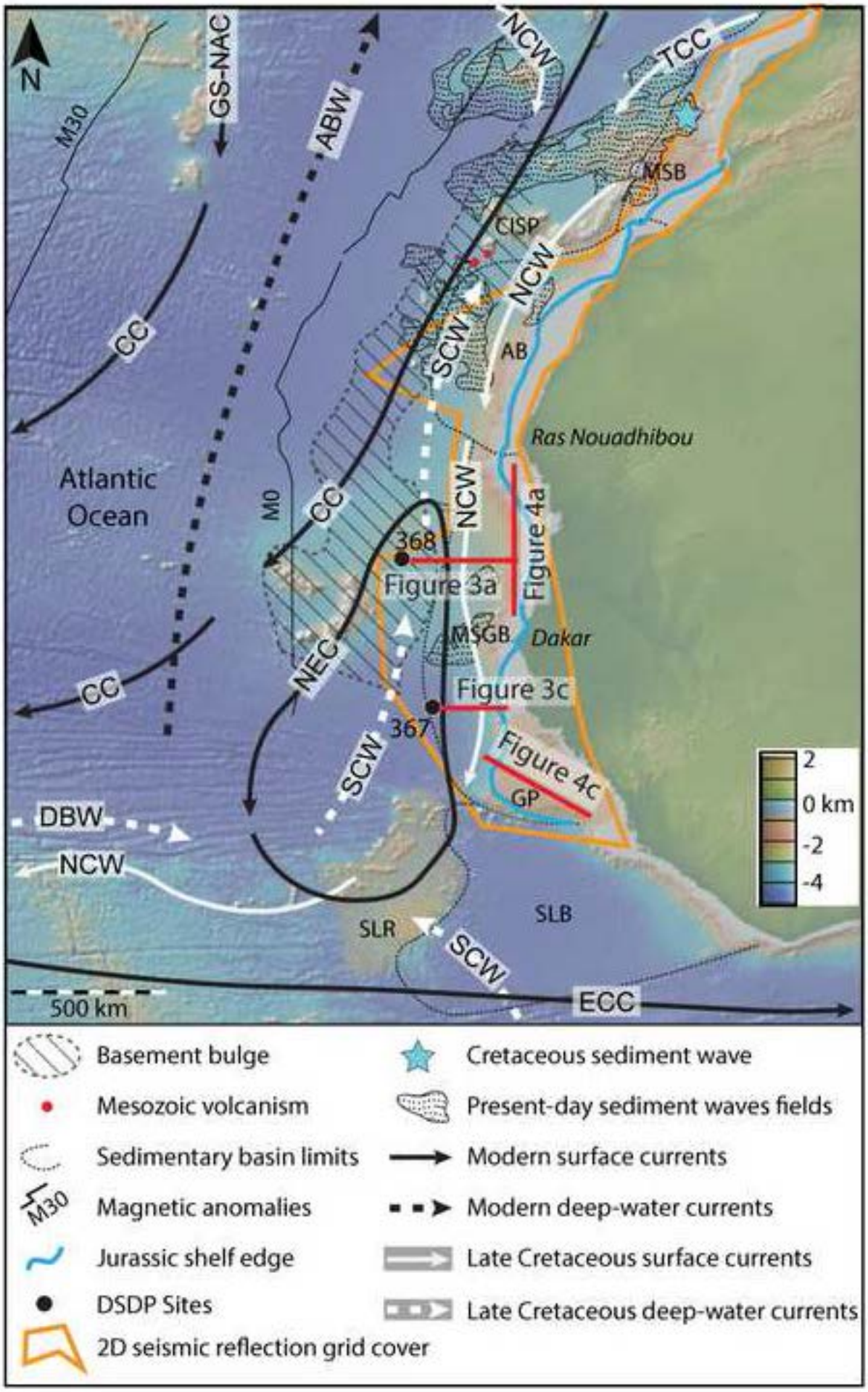

Figure 02

Click here to download high resolution image

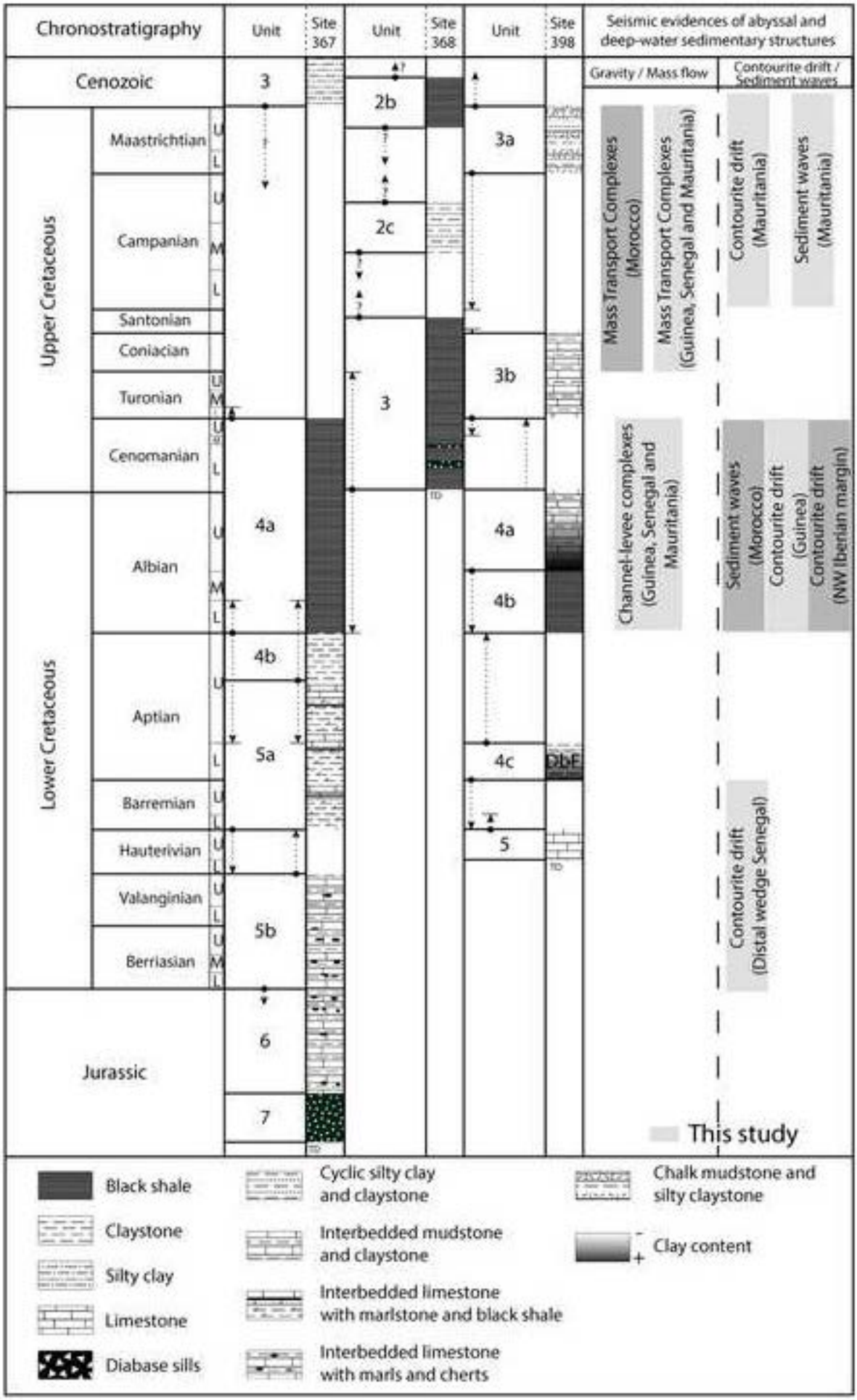

Figure 03
Click here to download high resolution image

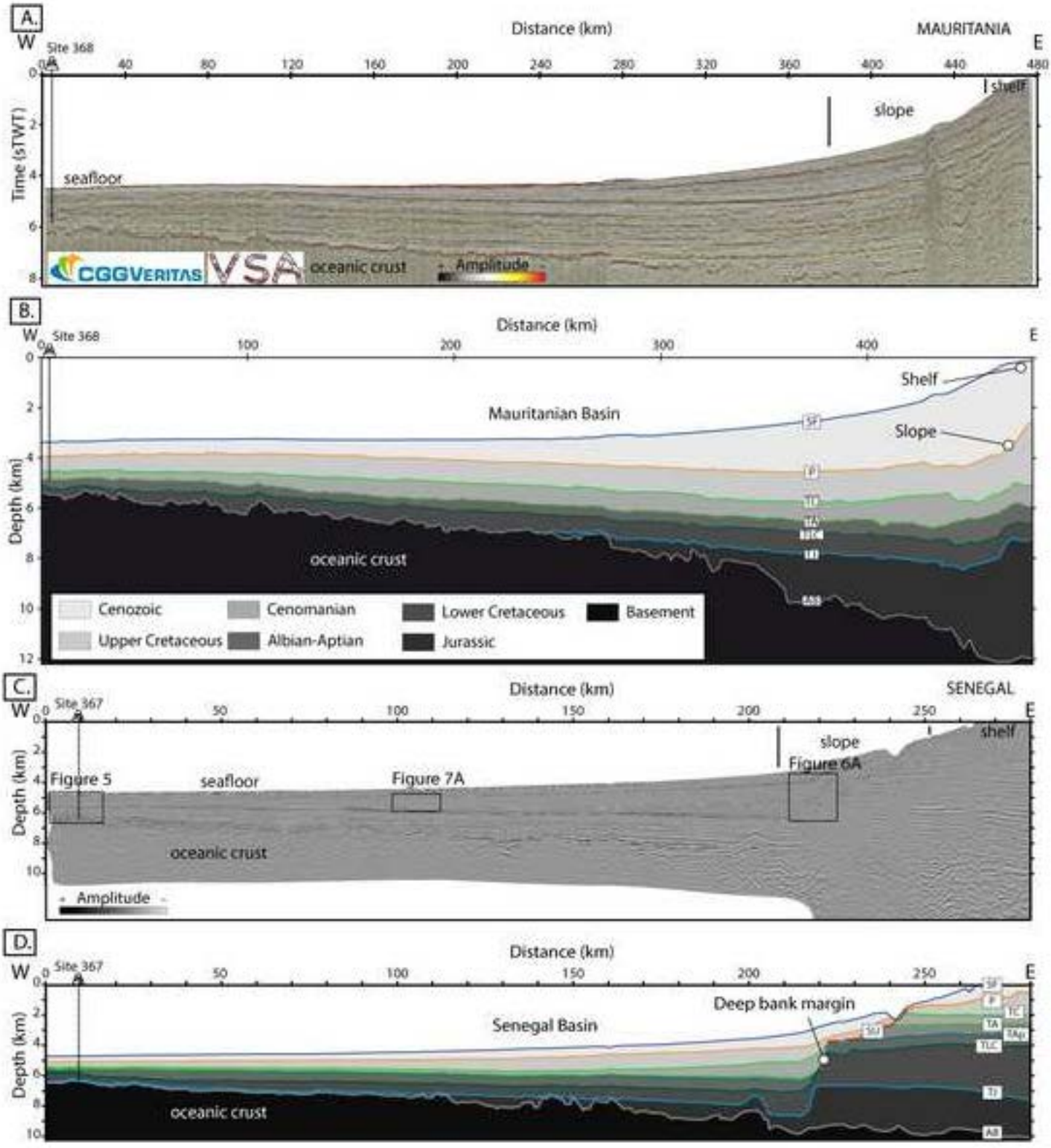

Figure 04

Click here to download high resolution image

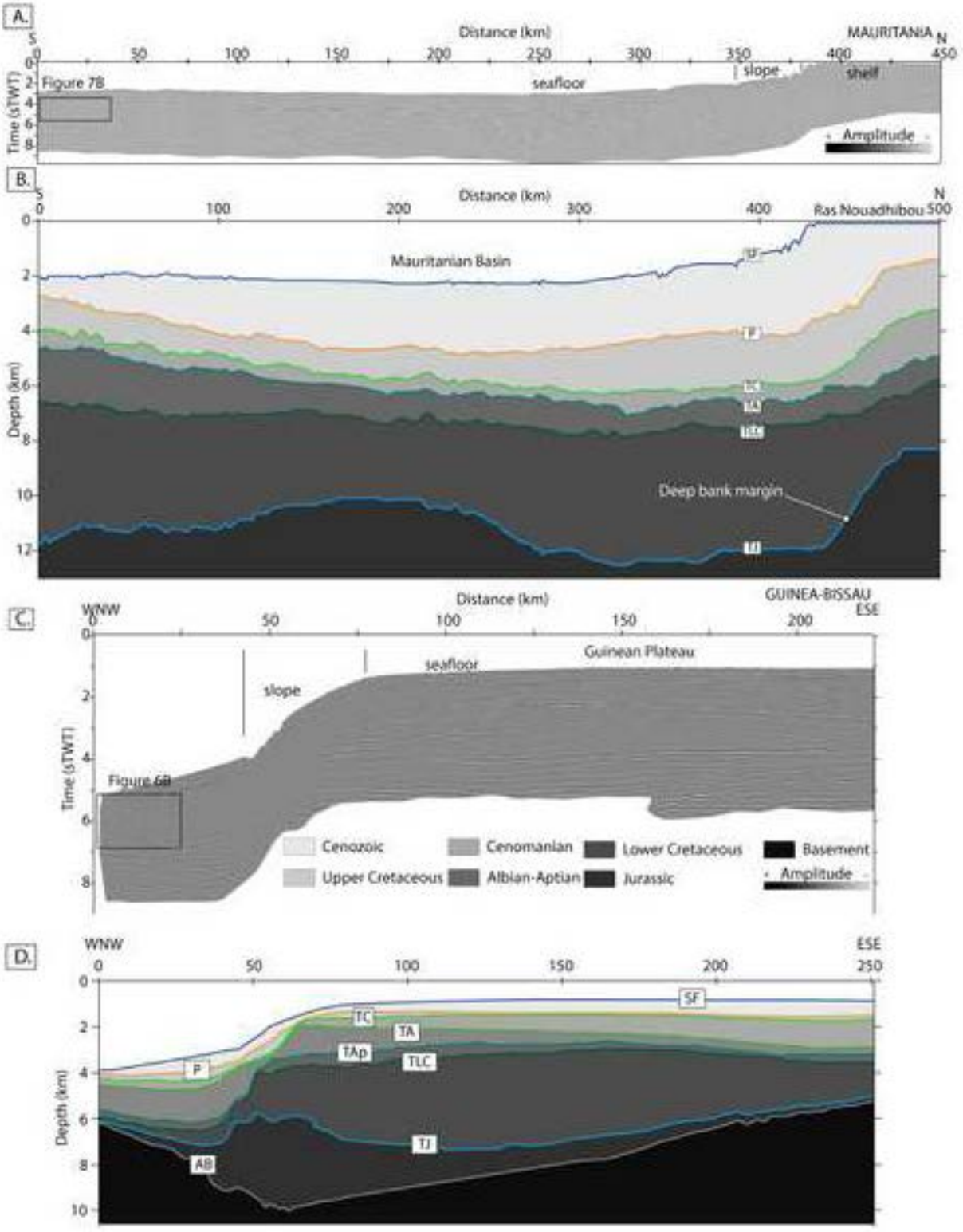

Figure 05
Click here to download high resolution image

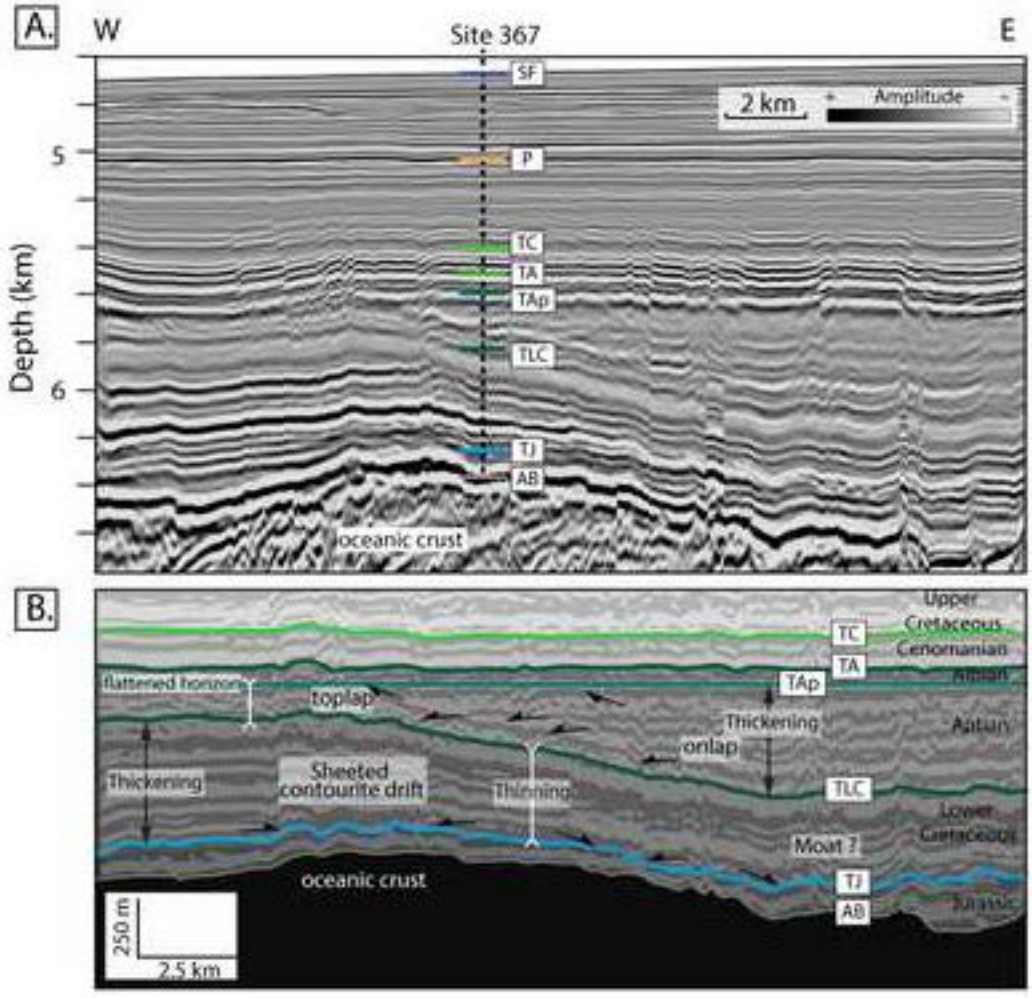

Figure 06
Click here to download high resolution image

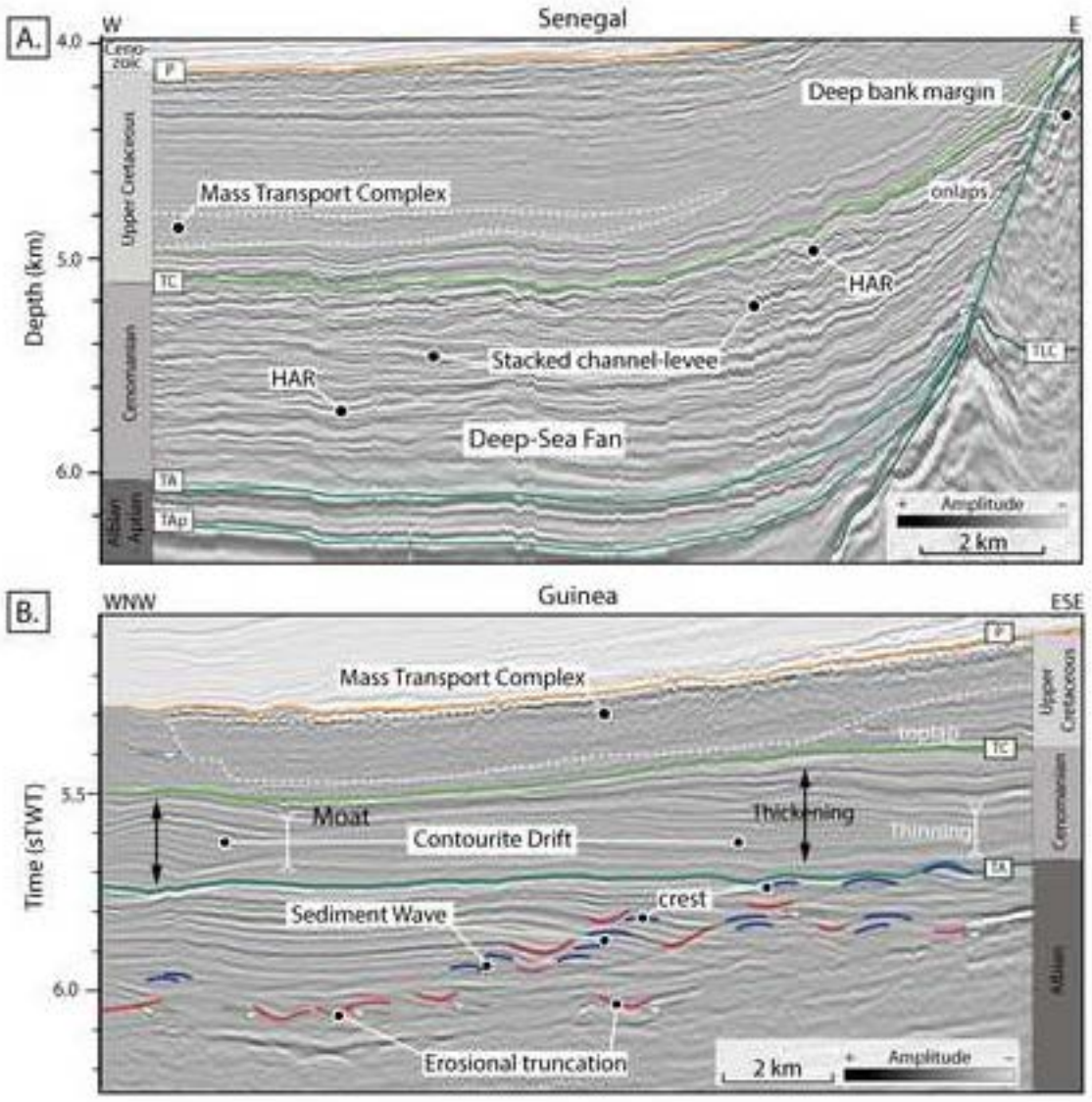

Figure 07
Click here to download high resolution image

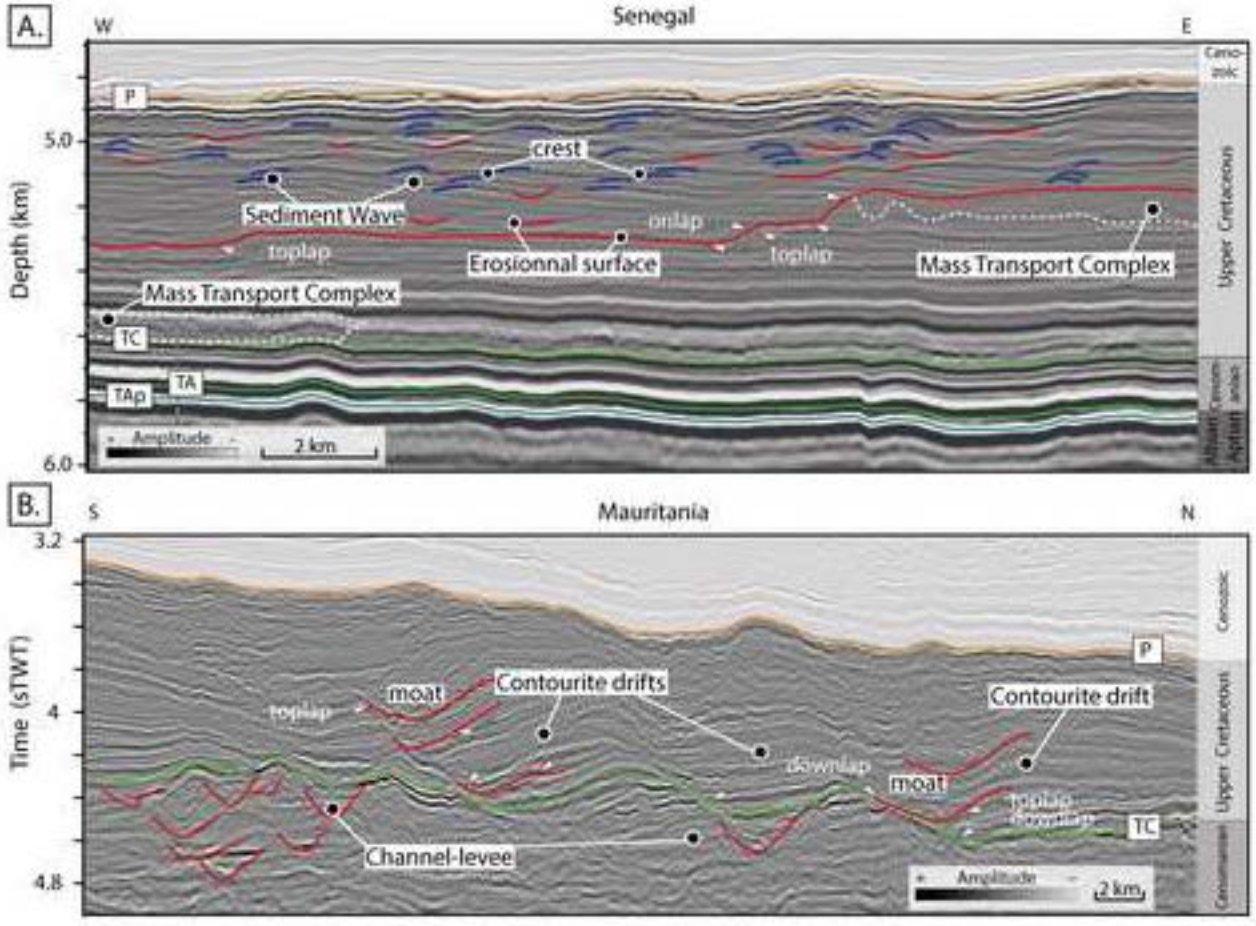

Figure 08
Click here to download high resolution image

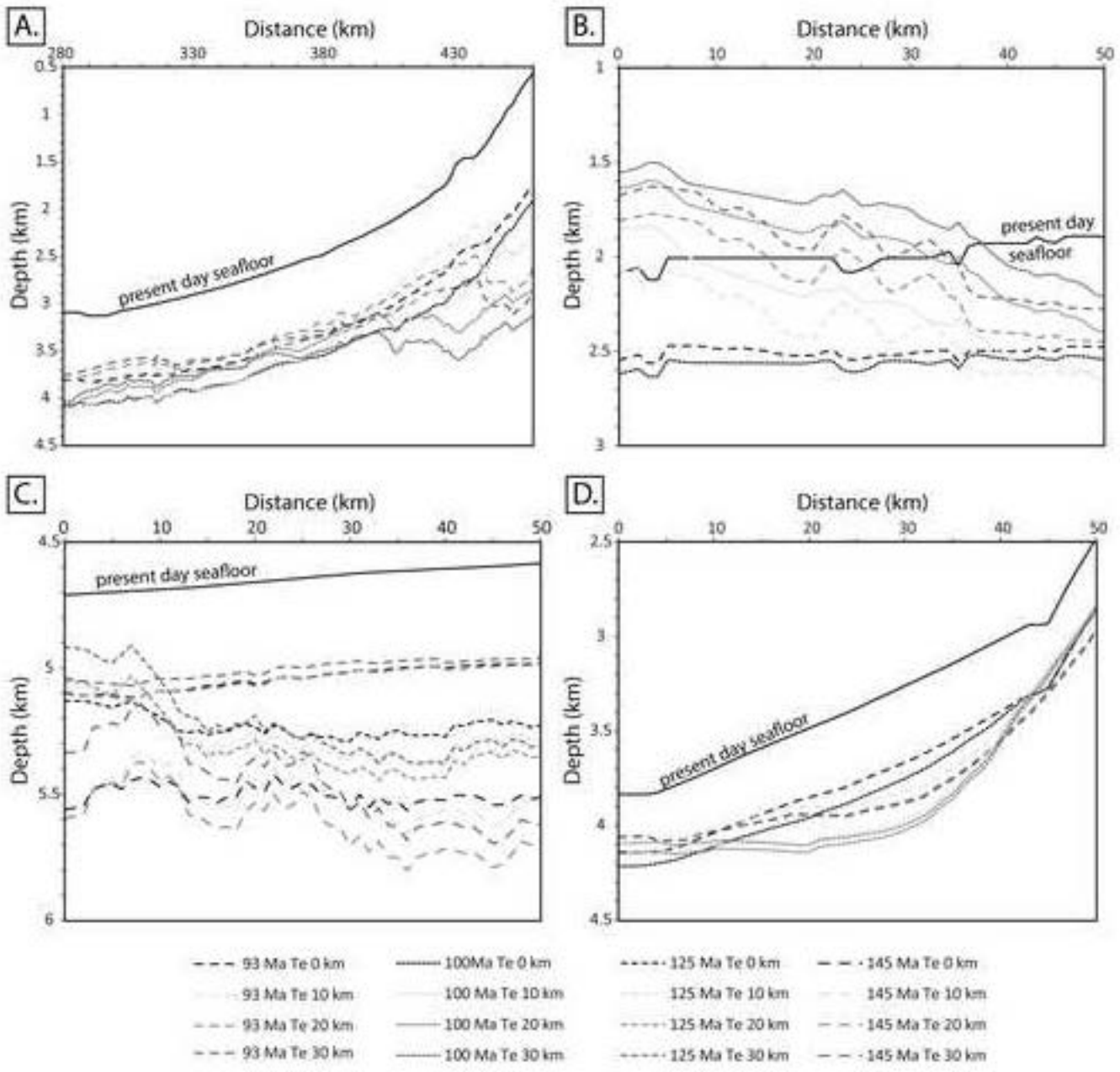

Figure 09
Click here to download high resolution image

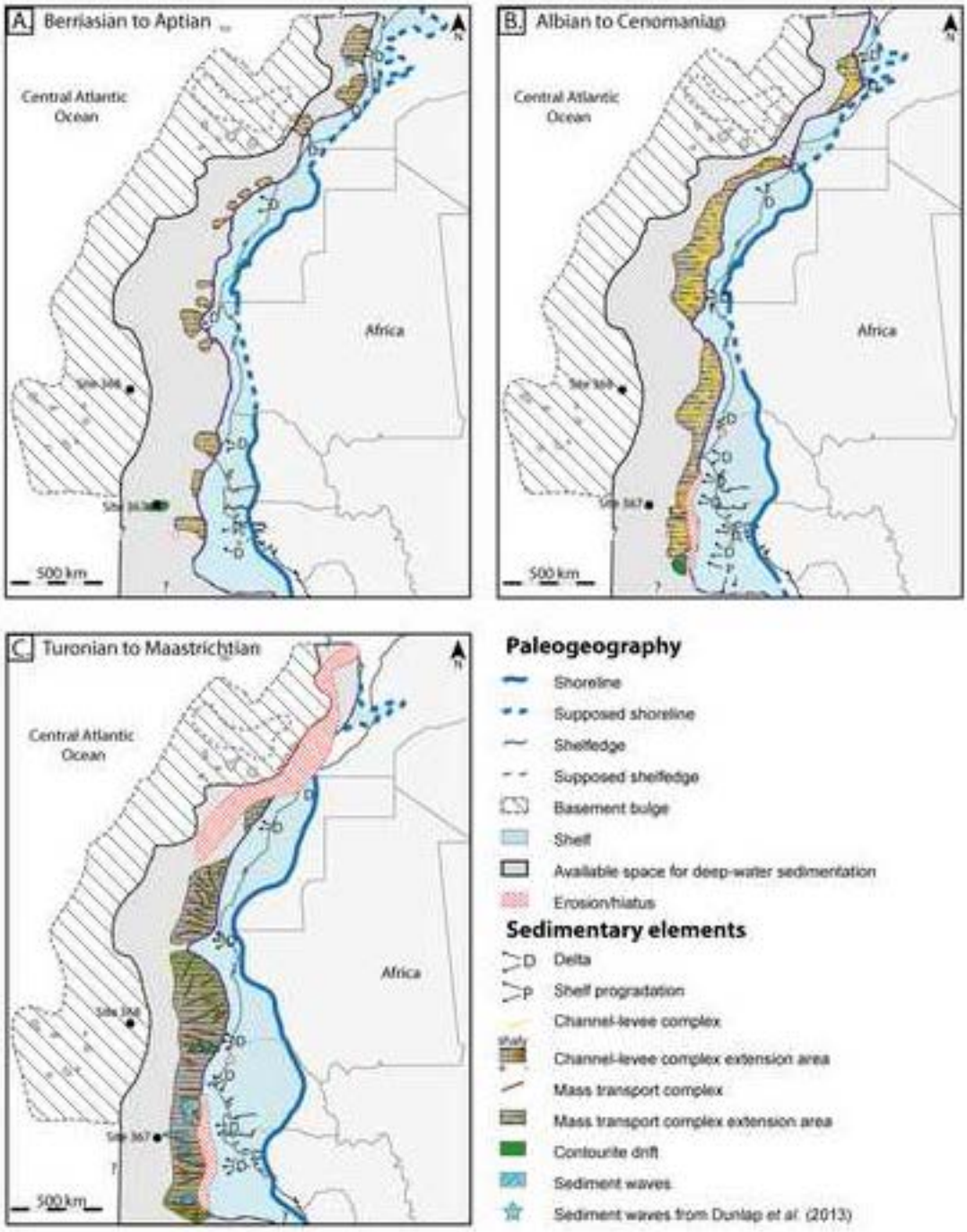

Figure 10
Click here to download high resolution image

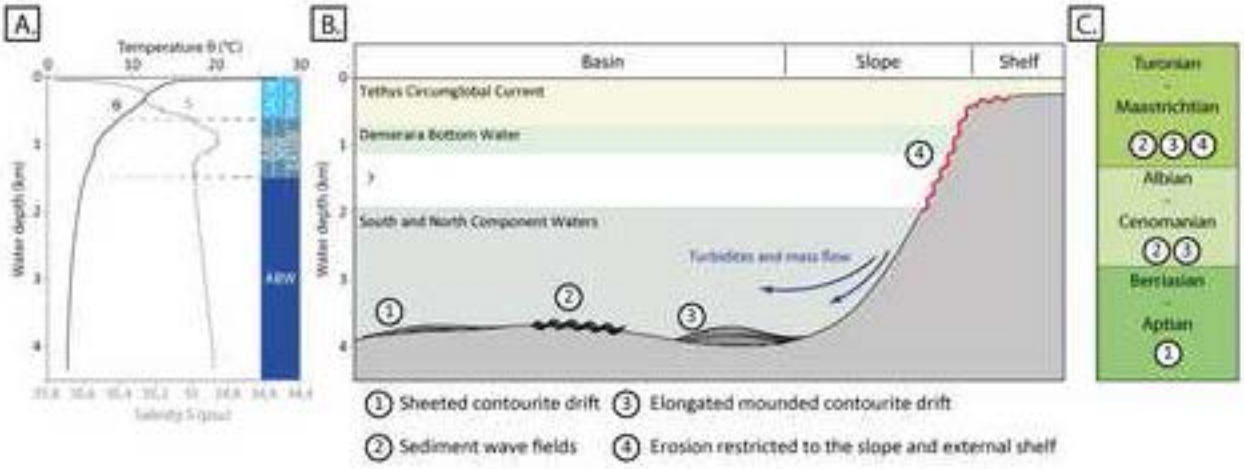

Table 01

Click here to download Table: Table 1_Mourlot-etal-EPSL-2017.xlsx

Section	Figure	Stratigraphic interval	Age (Ma)	Porosity (%)	Density (g/cc)	Lithology			
						% Sand	% Shaly sand	% Shale	% Limestone
Mauritania Basin	3A	Base Cenozoic to present-day seafloor	65 to 0	58.5	2.69	43	10	15	32
		Top Cenomanian to base Cenozoic	93 to 65	59.5	2.68	32	16	22	30
		Top Albian to top Cenomanian	100 to 93	58.1	2.68	50	0	20	30
		Top Lower Cretaceous to top Albian	125 to 100	59.5	2.68	30	30	0	40
		Top Jurassic to top Lower Cretaceous	145 to 125	55.3	2.67	40	45	0	15
		Top acoustic basement to top Jurassic	170 to 145	69.3	2.71	0	0	10	90
Senegal Basin	3C	Base Cenozoic to present-day seafloor	65 to 0	66.8	2.71	10	0	15	75
		Top Cenomanian to base Cenozoic	93 to 65	57.7	2.69	45	0	40	15
		Top Albian to top Cenomanian	100 to 93	65.6	2.70	13	0	23	64
		Top Aptian to top Albian	112 to 100	64.4	2.70	15	0	35	50
		Top Lower Cretaceous to top Aptian	125 to 112	66.5	2.71	10	0	20	70
		Top Jurassic to Lower Cretaceous	145 to 125	63.0	2.70	7	25	28	40
		Top acoustic basement to top Jurassic	170 to 145	69.3	2.71	0	0	10	90
Mauritania Basin	4A	Base Cenozoic to present-day seafloor	65 to 0	58.5	2.68	43	10	15	32
		Top Cenomanian to base Cenozoic	93 to 65	59.5	2.69	32	16	22	30
		Top Albian to top Cenomanian	100 to 93	58.1	2.68	50	0	20	30
		Top Aptian to top Albian	112 to 100	59.5	2.68	45	50	0	5
		Top Lower Cretaceous to top Aptian	125 to 112	55.3	2.67	30	30	0	40
		Top Jurassic to top Lower Cretaceous	145 to 125	69.3	2.71	0	0	10	90
Guinean Plateau	4C	Base Cenozoic to present-day seafloor	65 to 0	64.0	2.71	10	0	50	40
		Top Cenomanian to base Cenozoic	93 to 65	62.0	2.72	5	0	90	5
		Top Albian to top Cenomanian	100 to 93	64.0	2.72	0	0	80	20
		Top Aptian to top Albian	112 to 100	55.0	2.68	55	5	35	5
		Top Lower Cretaceous to top Aptian	125 to 112	64.0	2.72	20	0	20	60
		Top Jurassic to Lower Cretaceous	145 to 125	63.0	2.70	7	25	28	40
		Top acoustic basement to top Jurassic	170 to 145	69.0	2.17	0	0	10	90